NASA
Technical
Paper
2776

July 1988

NASA-TP-2776 19880015239

Nonlinear Programming Extensions to Rational Function Approximation Methods for Unsteady Aerodynamic Forces

Sherwood H. Tiffany
and William M. Adams, Jr.

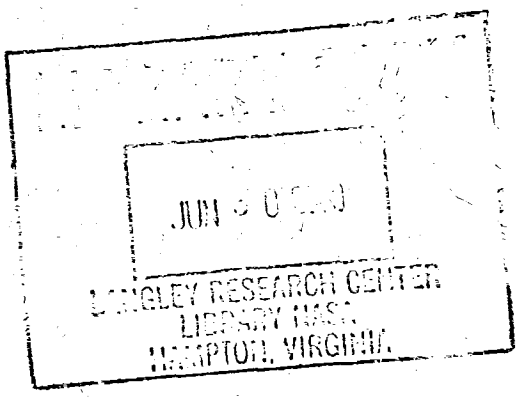

NASA

NASA Technical Paper 2776

1988

Nonlinear Programming Extensions to Rational Function Approximation Methods for Unsteady Aerodynamic Forces

Sherwood H. Tiffany
and William M. Adams, Jr.

Langley Research Center
Hampton, Virginia

National Aeronautics
and Space Administration

Scientific and Technical
Information Division

Abstract

This paper deals with approximating unsteady generalized aerodynamic forces in the equations of motion of a flexible aircraft. Two methods of formulating these approximations are extended to include both the same flexibility in constraining the approximations and the same methodology in optimizing nonlinear parameters as another currently used "extended least-squares" method. Optimal selection of "nonlinear parameters" is made in each of the three methods by use of the same nonlinear, nongradient optimizer. The objective of the nonlinear optimization is to obtain rational approximations to the unsteady aerodynamic forces whose state-space realization is lower order than that required when the nonlinear terms are not optimized. The free "linear parameters" are determined using least-squares matrix techniques. Selected linear equality constraints are solved explicitly or included implicitly, using a Lagrange multiplier formulation. State-space mathematical models resulting from the different approaches are described, and comparative evaluations are presented from application of each of the extended methods to a numerical example. The results obtained for the example problem show that the number of differential equations used to represent the unsteady aerodynamic forces in linear time-invariant equations of motion can be significantly reduced (up to 67 percent) from the number required by a conventional method in which nonlinear terms are not optimized.

1. Introduction

The equations of motion of a flexible aircraft contain unsteady generalized aerodynamic force terms which when expressed in the Laplace domain are transcendental functions. The availability of efficient linear systems algorithms for aeroservoelastic analysis and design has provided strong motivation to approximate the unsteady aerodynamic forces as rational functions of the Laplace variable (refs. 1–5). Such rational function approximations (RFA's) allow the aeroservoelastic equations of motion to be cast in a linear time-invariant (LTI) state-space form, although the size of the state vector increases due to the RFA's. This increased number of states due to the RFA's is referred to as the aerodynamic dimension. There is always a trade-off between how well the RFA's approximate the aerodynamic forces and how small the aerodynamic dimension can be kept.

The RFA formulations in the literature (e.g., refs. 1–11) have varying capabilities to perform such a trade-off. The purposes of this paper are (1) to place existing RFA approaches on an equal footing with respect to constraint imposition and the optimization algorithms employed and (2) to compare their performance.

Currently there are three basic formulations used in approximating unsteady generalized aerodynamic forces for arbitrary motion using rational functions:

1. Least-squares (LS)—references 2 and 5
2. Modified matrix-Padé (MMP)—references 3, 4, 6, and 7
3. Minimum-state (MS)—reference 8

For each of these rational function formulations, "best" approximations are determined, in a least-squares sense, to tabulated unsteady generalized aerodynamic force data.

An extended LS approach (ELS) was developed (refs. 9–11) which includes the capability of enforcing selected equality constraints on the RFA's and of optimizing the denominator coefficients in the rational functions with a nonlinear, nongradient optimizer (refs. 12–14). In this paper, the MMP approach of reference 6 and the MS approach of reference 8 are extended in a similar fashion. The extended approaches are referred to as "extended modified matrix-Padé" (EMMP) and "extended minimum-state" (EMS) approaches. The extensions bring them to the same level and flexibility in selecting constraints as the ELS approach of reference 9 and allow comparative evaluation using the same nongradient optimization techniques. Specifically,

1. The approach of reference 6 is generalized to include the same constraint selection as employed in reference 9.
2. The approach of reference 8 is generalized to allow more flexibility in the selection of constraints.
3. Both are altered so as to use the nongradient, nonlinear optimizer used in reference 9 in the constrained optimization of the free "nonlinear parameters" in each rational aerodynamic approximation.
4. All three use the same overall measure of relative error as a cost function for the nonlinear optimization; the necessity of normalizing the original aerodynamic data is essentially eliminated.

The "linear parameters" are determined by solving the equations of the least-squares problem with matrix techniques. Equality constraints are either included by using a Lagrange multiplier formulation of the equations or solved explicitly. Inequality constraints are included in the nonlinear optimization process.

The basic problems involved in approximating unsteady aerodynamic forces and methods used to solve them are presented in this paper. State-space

mathematical models resulting from the different approaches are described. Results obtained from application of the three extended methods to a numerical example are presented. Compared are the actual fits obtained, frequency responses for the corresponding systems of equations, and the total approximation error as a function of aerodynamic dimension. In addition some of the difficulties incurred in optimizing for the approximation parameters are discussed.

It is shown that all three extended approaches, ELS, EMMP, and EMS, demonstrate marked improvement over a baseline constrained, least-squares case in which nonlinear terms are not optimized. Furthermore, it is shown that both the EMMP and the EMS approximations compare favorably with the ELS approximations but with significant reductions in aerodynamic dimension. The corresponding aerodynamic dimension of the EMMP approach is approximately three-fourths that of the ELS approach, and the dimension of the newer EMS approach is approximately one-third that of ELS. However, the example selected had only one more input creating the aerodynamic forces (namely, incremental angle of attack due to vertical gust) than the number of generalized coordinates. For a case in which the difference between the number of inputs creating aerodynamic forces and the number of generalized coordinates is even larger (such as would occur for multiple control surfaces with irreversible actuators), the difference in aerodynamic dimension between the EMMP and ELS formulations would not be as significant. The basis for this statement is developed in the paper.

The software implementation of these RFA methods was developed to enhance the aeroservoelastic analysis capability of the ISAC (Interaction of Structures, Aerodynamics, and Controls) system of programs (ref. 15) and exists as an independent module in that system. Papers which describe other modules may be found by employing ISAC as a key word in a library search.

2. Approximating Unsteady Aerodynamic Forces

This section discusses the problems associated with using tabular unsteady aerodynamic force data in the study of stability and transient response characteristics and some methods used to solve them. Section 2.1 is a review of the equations of motion. Section 2.2 discusses the unsteady generalized aerodynamic forces and aeroelastic modeling. Section 2.3 discusses the rational function form used to approximate the aerodynamic forces, and section 2.4 presents a discussion of the constraints used to improve the reliability of the models in critical frequency regions.

2.1. Equations of Motion

Unsteady aerodynamic effects as well as structural dynamics must be considered when modeling flexible aircraft. A commonly employed approach to formulating the equations of motion for an elastic vehicle is based on a chosen number of vehicle vibration modes and Lagrange energy equations. Only small perturbations from a level equilibrium flight condition are considered herein. The perturbed aircraft is then represented by a linearized system of equations expressed in terms of generalized coordinates $\xi_i(t)$ as explained in reference 16. Through separation of variables the elastic deformation of the wing $z(x,y,t)$ can be represented by the sum of products of a finite set of shape functions $z_i(x,y)$ called mode shapes, and the $\xi_i(t)$ as

$$z(x,y,t) = \sum_{i=1}^{n_\xi} [z_i(x,y)\,\xi_i(t)] \tag{2.1}$$

The equations of motion (EOM) can then be formulated in the time domain as

$$\begin{aligned}\mathbf{M}\,\ddot{\boldsymbol{\xi}}(t) + \mathbf{G}\,\dot{\boldsymbol{\xi}}(t) + \mathbf{K}\,\boldsymbol{\xi}(t) \\ = q\,[\mathbf{F}_\xi(t) + \mathbf{F}_g(t)] + \mathbf{F}_\delta(t)\end{aligned} \tag{2.2}$$

where

q	dynamic pressure
$\mathbf{M}, \mathbf{K}$	generalized mass and stiffness matrices
$\mathbf{G}$	damping coefficient matrix where the structural damping is modeled as viscous
$\mathbf{F}_\xi$	matrix of aerodynamic forces due to aircraft and control surface motions
$\mathbf{F}_g$	vector of aerodynamic forces due to gusts
$\mathbf{F}_\delta$	vector of generalized forces due to the controls
$\mathbf{F}$	$= \left[\mathbf{F}_\xi \,\middle|\, \mathbf{F}_g\right]$, partitioned matrix of aerodynamic forces

Equation (2.1) when transformed into the Laplace domain can be written as

$$\begin{aligned}[\mathbf{M}s^2 + \mathbf{G}s + \mathbf{K} - q\mathbf{Q}_\xi]\tilde{\boldsymbol{\xi}}(s) \\ = q\mathbf{Q}_g\alpha_g + \mathbf{F}_{\mathrm{HM}}\mathbf{T}_{\mathrm{HM}}\end{aligned} \tag{2.3}$$

where

$\mathbf{Q}_\xi$ matrix of aerodynamic force coefficients due to aircraft and control surface motions, equal to $[Q_{ij}(s)]$, for $i = 1, \ldots, n_\xi$ and $j = 1, \ldots, n_\xi$

$\mathbf{Q}_g$ matrix of aerodynamic forces due to gusts, equal to $[Q_{ij}(s)]$, for $i = 1, \ldots, n_\xi$ and $j = n_\xi + 1, \ldots, n_\xi + n_g$

α_g nondimensional gust velocities, $\{w_g/u \quad v_g/u\}^T$

$\mathbf{F}_{\mathrm{HM}}$ $n_\xi \times n_\delta$ matrix of modal coefficients converting hinge-moment outputs to generalized forces

$\mathbf{T}_{\mathrm{HM}}$ vector of hinge moments output by actuator (note that $\mathbf{T}_{\mathrm{HM}}$ is typically a function of actuator characteristics, backup structure stiffness, and control law feedback; for this paper, identification of the additional dynamics and interconnections is suppressed)

$\mathbf{Q} = \left[\mathbf{Q}_\xi \mid \mathbf{Q}_g\right]$, matrix of generalized aerodynamic force coefficients

It is the matrix $\mathbf{Q}$ of force coefficients which is of interest in this paper. Each element Q_{ij} of $\mathbf{Q}$ is defined as

$$Q_{ij}(s) = \iint_S \frac{\Delta P_j(x, y, s)}{q} z_i(x, y)\, dS \qquad (2.4)$$

Here $\Delta P_j(x, y, s)$ is the pressure difference due to motion in the jth generalized coordinate.

Rational function approximations (RFA) allow the aeroservoelastic equations of motion to be cast in an LTI state-space form for which a large number of efficient linear systems algorithms are available:

$$\dot{\chi} = \mathbf{A}\chi + \mathbf{B}\mathbf{U} \qquad (2.5)$$

where

χ vector of states

$\mathbf{U}$ vector of inputs

$\mathbf{A}, \mathbf{B}$ matrix multipliers

Thus there is strong motivation for approximating the unsteady generalized aerodynamic forces (GAF's) as rational functions of the Laplace variable (refs. 1–5). Subsequent sections describe the steps required to obtain the RFA's.

2.2. Generalized Aerodynamic Forces and Aeroelastic Modeling

This section sets the stage for obtaining the RFA's of the generalized aerodynamic forces by stating how the GAF's are currently generated, by indicating the condition for which the GAF's are desired, and by introducing the approach that is employed to approximate the desired representation.

2.2.1. Oscillatory motion. Using such techniques as doublet-lattice or kernel function theories (refs. 17 and 18), programs currently available for generation of unsteady GAF's can compute the forces only for purely oscillatory motion over a range of specified values of reduced frequency. Consequently, the GAF's are not defined as explicit functions of k, but are defined only as tabular functions and are transcendental. Using these tabular functions, iterative methods must necessarily be used to determine eigenvalues of the flexible aircraft equations of motion. These iterative methods tend to be costly, and the solutions are exact only for purely oscillatory motion. Most importantly, LTI methods cannot be used.

2.2.2. Arbitrary motion. In order to obtain solutions in the Laplace domain for both growing and decaying motion (s off the $i\omega$-axis), it is necessary to express the forces as functions of s for the entire complex s-plane, or equivalently for the nondimensionalized complex p-plane. In lieu of developing new aerodynamic theory, the concept of analytic continuation is often used to justify extending these functions, which are defined only on the frequency axis ($s = i\omega$), to the entire complex plane by finding analytic functions which agree with the aerodynamic forcing functions at all values of frequency. However, there are only a finite number of frequencies at which tabular data are available; hence, this process is at best an approximate analytic continuation into the region near the portion of the axis containing the tabular data. Since phenomena such as flutter occur for points in the complex s-plane which lie along the $i\omega$-axis, approximations into the region near the axis are sufficient for most studies.

Figure 1 depicts the approximating process, where

k reduced frequency

p nondimensionalized Laplace variable

$Q_{ij}(ik_n)$ reduced-frequency domain tabular data (identified by the open circles)

$\hat{Q}_{ij}(ik)$ approximating curve, $\hat{Q}_{ij}(p)$ for $p = ik$ (corresponding to the solid line)

$\hat{Q}_{ij}(ik_n)$ points along the approximating curve at reduced frequencies k_n corresponding to the tabular data (solid circles)

$\varepsilon_{ij}(ik_n)$ approximation error between two corresponding points (denoted by an arrow between points)

2.3. Rational Function Approximations to Generalized Aerodynamic Forces

The most common form of the approximating functions used currently for each generalized force coefficient Q_{ij} of $\mathbf{Q}$ is a rational function of the nondimensional Laplace variable p. Each can be expressed in the following partial fraction form, where n_L is the number of partial fractions (referred to herein as the "order of fit"), which is equivalent to the order of the overall denominator polynomial:

$$\hat{Q}_{ij}(p) = (A_0)_{ij} + (A_1)_{ij}p + (A_2)_{ij}p^2 + \sum_{\ell=1}^{n_L}(A_{\ell+2})_{ij}\frac{p}{p+b_\ell} \tag{2.6}$$

which can be rewritten as

$$\hat{Q}_{ij}(s) = (\bar{A}_0)_{ij} + (\bar{A}_1)_{ij}s + (\bar{A}_2)_{ij}s^2 + \sum_{\ell=1}^{n_L}(\bar{A}_{\ell+2})_{ij}\frac{s}{s+\bar{b}_\ell} \tag{2.7}$$

where

$$p = \frac{c}{2u}s$$

$$\bar{b}_\ell = \frac{2u}{c}b_\ell$$

$$\bar{A}_0 = A_0$$

$$\bar{A}_1 = \frac{c}{2u}A_1$$

$$\bar{A}_2 = \left(\frac{c}{2u}\right)^2 A_2$$

$$\bar{A}_{\ell+2} = A_{\ell+2}$$

The partial fractions are commonly called lag terms because each represents a transfer function in which the output "lags" the input and permits an approximation of the time delays inherent in unsteady aerodynamics (ref. 5). Because tabular data are determined for specified values of reduced frequency k_n the Q_{ij} are actually defined only for values of the nondimensionalized Laplace variable $p = ik_n$. Variations in the matrix form of the rational functions result in three currently used approaches, mentioned in the introduction, to approximating the unsteady aerodynamic force coefficients.

2.4. Constraints

It is often desirable to impose constraints on the approximating functions. For instance, one might wish that the approximating functions agree with the tabular data at the steady-state conditions (e.g., $\hat{Q}_{ij} = Q_{ij}$ at $k = 0$). Without constraints imposed, as depicted in figure 2(a), the fit at zero frequency can be poor, although the overall shape of the approximating curve may be good. Figures 2(a) and 2(b) depict the "steady-state area" (within a shaded box) where constraints might be imposed. In some instances, agreement of the slopes of the curves at a specified frequency might be necessary. For critical flutter modes, it might be desirable to impose agreement between computed data and the approximating functions near the flutter frequency. When constraints are imposed, there is a corresponding loss in degrees of freedom for the least-squares solution. The possible change in the approximating curve due to this loss is also depicted in figure 2(b).

The standard method of improving the fits, especially when constraints have been imposed, is to increase the order of fit used in the approximation (i.e., make n_L in eq. (2.7) larger) or to decrease the frequency range of the approximations. In recent years, methods have been developed to improve these RFA's by optimally selecting certain nonlinear coefficients via nonlinear programming techniques (refs. 6–9). These studies indicate the advantages of optimizing the nonlinear coefficients not only to reduce the error for a given order of fit, but also to provide a way of reducing the order of fit required to achieve a specified level of error. These concepts are explored and extended in this paper.

3. Matrix Formulations of Rational Function Approximations and Their Corresponding State-Space Equations

There are several variations on the matrix form of the rational function approximations for the unsteady aerodynamic force coefficients corresponding

to the LS, the MMP, and the MS formulations. Each matrix formulation results in different aerodynamic state vectors. The mathematical models for each of the three main variations on the matrix form of the rational functions and their corresponding state-space equations are defined in this section. Section 3.1 presents the equations for the least-squares RFA formulation as developed by the authors and used in the comparisons presented in this paper. Section 3.2 defines the equations for the modified matrix-Padé RFA formulation, and section 3.3 defines those for the minimum-state RFA formulation.

3.1. Least-Squares (Column-Independent) RFA Formulation

Historically, Roger (ref. 2) and, later, Abel (ref. 5) formulated the rational function approximations so as to use the same denominator coefficients for all the elements Q_{ij} of the matrix $\mathbf{Q}$ in order to reduce the number of aerodynamic states in an LTI form of the equations of motion. In effect, therefore, the formulation was "element-independent" with respect to the denominator coefficients. It is, nevertheless, referred to here as "column-independent" to distinguish it from the MMP approach of section 3.2.

The condition that each element Q_{ij} of $\mathbf{Q}$ has the same constant denominator coefficients, or lag coefficients, b_ℓ, allows the "per element" expressions of equation (2.6) to be valid for the full matrix $\mathbf{Q}$:

$$\hat{\mathbf{Q}}(p) = \left[\hat{\mathbf{Q}}_\xi(p) \,\middle|\, \hat{\mathbf{Q}}_g(p)\right] = \mathbf{A}_0 + \mathbf{A}_1 p + \mathbf{A}_2 p^2 + \sum_{\ell=1}^{n_L} \mathbf{A}_{\ell+2} \frac{p}{p + b_\ell} \tag{3.1a}$$

which, when expressed in the Laplace s-domain, is:

$$\hat{\mathbf{Q}}(s) = \left[\hat{\mathbf{Q}}_\xi(s) \,\middle|\, \hat{\mathbf{Q}}_g(s)\right] = \bar{\mathbf{A}}_0 + \bar{\mathbf{A}}_1 s + \bar{\mathbf{A}}_2 s^2 + \sum_{\ell=1}^{n_L} \bar{\mathbf{A}}_{\ell+2} \frac{s}{s + \bar{b}_\ell} \tag{3.1b}$$

Each matrix in equations (3.1) is rectangular, with dimensions $n_\xi \times (n_\xi + n_g)$. To develop a state-space realization for equation (2.3), $\mathbf{Q}(s)$ is approximated by $\hat{\mathbf{Q}}(s)$, as defined in equation (3.1b), giving

$$\begin{aligned} &\left\{\mathbf{M}s^2 + \mathbf{G}s + \mathbf{K} - q\left[(\bar{\mathbf{A}}_0)_\xi + (\bar{\mathbf{A}}_1)_\xi s + (\bar{\mathbf{A}}_2)_\xi s^2 + \sum_{\ell=1}^{n_L} (\bar{\mathbf{A}}_{\ell+2})_\xi \frac{s}{s + \bar{b}_\ell}\right]\right\} \tilde{\boldsymbol{\xi}}(s) \\ &\quad = \mathbf{F}_{\mathrm{HM}} \mathbf{T}_{\mathrm{HM}} + q\left[(\bar{\mathbf{A}}_0)_g + (\bar{\mathbf{A}}_1)_g s + (\bar{\mathbf{A}}_2)_g s^2 + \sum_{\ell=1}^{n_L} (\bar{\mathbf{A}}_{\ell+2})_g \frac{s}{s + \bar{b}_\ell}\right] \boldsymbol{\alpha}_g \end{aligned} \tag{3.2a}$$

If the aerodynamic states are defined by

$$X_{a_\ell} = \frac{s}{s + \bar{b}_\ell} \begin{Bmatrix} \hat{\boldsymbol{\xi}} \\ \boldsymbol{\alpha}_g \end{Bmatrix} \qquad (\text{For } \ell = 1, \ldots, n_L) \tag{3.2b}$$

there would be $(n_\xi + n_g) \times n_L$ aerodynamic states in the LTI state-space form (eq. (2.5)).

3.1.1. LS RFA aerodynamic dimension reduction. An alternative formulation of the aerodynamic states described below significantly reduces the number of aerodynamic states when n_g is nonzero. This modification uses a definition for the aerodynamic states which combines the elastic and gust modes.

Equation (3.2) is equivalent to

$$\left\{[\mathbf{M}-q(\bar{\mathbf{A}}_2)_\xi]s^2+[\mathbf{G}-q(\bar{\mathbf{A}}_1)_\xi]s+[\mathbf{K}-q(\bar{\mathbf{A}}_0)_\xi]\right\}\tilde{\boldsymbol{\xi}}(s)-q\sum_{\ell=1}^{n_L}\left\{\left[(\bar{\mathbf{A}}_{\ell+2})_\xi \,\middle|\, (\bar{\mathbf{A}}_{\ell+2})_g\right]\frac{s}{s+\bar{b}_\ell}\begin{Bmatrix}\tilde{\boldsymbol{\xi}}\\ \boldsymbol{\alpha}_g\end{Bmatrix}\right\}$$
$$=\mathbf{F}_{\mathrm{HM}}\mathbf{T}_{\mathrm{HM}}+q\left[(\bar{\mathbf{A}}_0)_g+(\bar{\mathbf{A}}_1)_g s+(\bar{\mathbf{A}}_2)_g s^2\right]\boldsymbol{\alpha}_g \tag{3.3a}$$

Hence, if the augmenting aerodynamic state vector $\mathbf{X}_a$ is defined by

$$\mathbf{X}_a=\begin{bmatrix}\mathbf{X}_{a_1} & \mathbf{X}_{a2} & \cdots & \mathbf{X}_{a_{n_L}}\end{bmatrix}^T$$

where each

$$\mathbf{X}_{a_\ell}=\left[(\bar{\mathbf{A}}_{\ell+2})_\xi \,\middle|\, (\bar{\mathbf{A}}_{\ell+2})_g\right]\frac{s}{s+\bar{b}_\ell}\begin{Bmatrix}\tilde{\boldsymbol{\xi}}\\ \boldsymbol{\alpha}_g\end{Bmatrix}=(\bar{\mathbf{A}}_{\ell+2})\frac{1}{s+\bar{b}_\ell}\boldsymbol{\eta}=\frac{1}{s+\bar{b}_\ell}(\bar{\mathbf{A}}_{\ell+2})\boldsymbol{\eta}=\frac{1}{s+\bar{b}_\ell}\boldsymbol{\eta}'_\ell \tag{3.3b}$$

and

$$\boldsymbol{\eta}=s\begin{Bmatrix}\tilde{\boldsymbol{\xi}}\\ \boldsymbol{\alpha}_g\end{Bmatrix}$$
$$\boldsymbol{\eta}'_\ell=(\bar{\mathbf{A}}_{\ell+2})\,\boldsymbol{\eta}\qquad(\text{For } \ell=1,\ \ldots,\ n_L)$$

then an LTI state-space realization for equations (3.3) is

$$s\mathbf{X}_{a_\ell}=-\bar{b}_\ell\mathbf{I}\mathbf{X}_{a_\ell}+\mathbf{I}\boldsymbol{\eta}'_\ell \tag{3.4}$$

or more explicitly

$$s\mathbf{X}_{a_\ell}=-\bar{b}_\ell\mathbf{I}\mathbf{X}_{a_\ell}+(\bar{\mathbf{A}}_{\ell+2})_\xi\, s\tilde{\boldsymbol{\xi}}+(\bar{\mathbf{A}}_{\ell+2})_g\, s\boldsymbol{\alpha}_g \tag{3.5}$$

Since $\bar{\mathbf{A}}_{\ell+2}$ is of size $n_\xi\times(n_\xi+n_g)$, each $\boldsymbol{\eta}'_\ell$ is of size n_ξ, so there are exactly n_ξ states for each $\ell=1,\ \ldots,\ n_L$. This implies that the number of added aerodynamic states for state-space realization of equation (2.3) due to the partial fractions (or lag terms) in equations (3.1) for this column-independent formulation is

$$n_a=n_\xi n_L \tag{3.6}$$

The state equations for the aeroelastic system for Roger's RFA formulation are obtained by substituting equation (3.3b) into equation (3.3a), converting to first order form, and then combining with equation (3.5). The resulting set of LTI state-space equations are

$$
s\begin{Bmatrix} \tilde{\xi} \\ s\tilde{\xi} \\ \mathbf{X}_a \end{Bmatrix} = \left[\begin{array}{c|c|c} \mathbf{I} & 0 & 0 \\ \hline 0 & \mathbf{M}-q(\bar{\mathbf{A}}_2)_\xi & 0 \\ \hline 0 & 0 & \mathbf{I} \end{array}\right]^{-1} \left[\begin{array}{c|c|c} 0 & \mathbf{I} & 0 \\ \hline -(\mathbf{K}-q(\bar{\mathbf{A}}_0)_\xi) & -(\mathbf{G}-q(\bar{\mathbf{A}}_1)_\xi) & q[\mathbf{I} \ \ldots \ \mathbf{I}] \\ \hline 0 & (\bar{\mathbf{A}}_3)_\xi & -\bar{b}_1\mathbf{I} \ \ldots \ 0 \\ \vdots & \vdots & \vdots \ \ddots \ \vdots \\ 0 & (\bar{\mathbf{A}}_{n_L+2})_\xi & 0 \ \ldots \ -\bar{b}_{n_L}\mathbf{I} \end{array}\right] \begin{Bmatrix} \tilde{\xi} \\ s\tilde{\xi} \\ \mathbf{X}_a \end{Bmatrix}
$$

$$
+ \left[\begin{array}{c|c|c} \mathbf{I} & 0 & 0 \\ \hline 0 & \mathbf{M}-q(\bar{\mathbf{A}}_2)_\xi & 0 \\ \hline 0 & 0 & \mathbf{I} \end{array}\right]^{-1} \left[\begin{array}{c|c|c|c} 0 & \mathbf{I} & 0 & 0 \\ \hline \mathbf{F}_{\mathrm{HM}} & q(\bar{\mathbf{A}}_0)_g & q(\bar{\mathbf{A}}_1)_g & q(\bar{\mathbf{A}}_2)_g \\ \hline 0 & 0 & (\bar{\mathbf{A}}_3)_g & 0 \\ \vdots & \vdots & \vdots & \vdots \\ 0 & 0 & (\bar{\mathbf{A}}_{(n_L+2)})_g & 0 \end{array}\right] \begin{Bmatrix} \mathbf{T}_{\mathrm{HM}} \\ \boldsymbol{\alpha}_g \\ s\boldsymbol{\alpha}_g \\ s^2\boldsymbol{\alpha}_g \end{Bmatrix} \tag{3.7}
$$

This formulation was used for most of the analyses reported in references 19–21.

3.1.2. LS RFA for irreversible actuators. For the column-independent LS formulation, a significant reduction in the aerodynamic dimension is possible if the actuators driving the control surfaces can be considered irreversible. In this case, the $n_{\delta'}$ inputs associated with control deflections are approximated as not being affected by aerodynamic and inertial cross-coupling hinge moments. Thus

$$
\delta' = \mathbf{T}_A(s)\delta'_c \tag{3.8}
$$

where

δ'_c	$n_{\delta'} \times 1$ vector of commanded control inputs
$\mathbf{T}_A(s)$	diagonal transfer matrix relating control deflections to commanded control inputs

Under this approximation, only the first $n_{\xi'}$ equations of (2.3) are needed since

$$
\tilde{\xi} = \begin{Bmatrix} \tilde{\xi}' \\ \delta' \end{Bmatrix} = \begin{Bmatrix} \tilde{\xi}' \\ \mathbf{T}_A\delta'_c \end{Bmatrix} \tag{3.9}
$$

and hence the rows defining the $n_{\delta'}$ deflections can be deleted, and terms in the first $n_{\xi'}$ equations involving δ' can be expressed in terms of commanded inputs. Thus the aerodynamic dimension for this case, using the LS formulation, is only

$$
n_a = n_{\xi'}n_L \tag{3.10}
$$

3.2. Modified Matrix-Padé (Column-Dependent) RFA Formulation

In the MMP approach, the denominator coefficients b_ℓ are fixed for all elements of a particular column, but their number and values may vary between columns; that is, they may be "column-dependent." Thus, for the MMP formulation, the per element expression (eq. (2.6)) holds only per column, not for the entire matrix **Q** as in equation (3.1):

$$\hat{\mathbf{Q}}_j(p) = (\mathbf{A}_0)_j + (\mathbf{A}_1)_j p + (\mathbf{A}_2)_j p^2 + \sum_{\ell=1}^{n_{L_j}} (\mathbf{A}_{\ell+2})_j \frac{p}{p + b_{\ell_j}} \tag{3.11}$$

The $\hat{\mathbf{Q}}_j(p)$ are then combined as

$$\hat{\mathbf{Q}}(p) = \mathbf{A}_0 + \mathbf{A}_1 p + \mathbf{A}_2 p^2 + [\mathbf{W}_1(p) \quad \dots \quad \mathbf{W}_{n_\xi + n_g}(p)] \begin{bmatrix} \frac{1}{h_1(p)} & \cdots & 0 \\ \vdots & \ddots & \vdots \\ 0 & \cdots & \frac{1}{h_{n_\xi + n_g}(p)} \end{bmatrix} p \tag{3.12a}$$

where

$$\mathbf{W}_j(p) = \sum_{\ell=1}^{n_{L_j}} (\mathbf{A}_{\ell+2})_j \prod_{\substack{k=1 \\ k \neq \ell}}^{n_{L_j}} (p + b_{k_j}) \tag{3.12b}$$

and

$$h_j(p) = \prod_{\ell=1}^{n_{L_j}} (p + b_{\ell_j}) \qquad (\text{For } j = 1, \ \dots, \ n_\xi + n_g) \tag{3.12c}$$

If the augmenting aerodynamic state vector,

$$\mathbf{X}_a = [\mathbf{X}_{a_1} \quad \mathbf{X}_{a_2} \quad \dots \quad \mathbf{X}_{a_{n_\xi + n_g}}]^T$$

is defined by

$$s\mathbf{X}_{a_j} = \begin{bmatrix} 0 & 1 & \cdots & 0 \\ \vdots & \vdots & \ddots & \vdots \\ 0 & 0 & \cdots & 1 \\ -\bar{h}_{j1} & 0 & \cdots & -\bar{h}_{jn_{L_j}} \end{bmatrix} \mathbf{X}_{a_j} + \begin{pmatrix} 0 \\ \vdots \\ 0 \\ 1 \end{pmatrix} \eta \tag{3.13a}$$

$$= \bar{\mathbf{H}}_j \mathbf{X}_{a_j} + \bar{\mathbf{V}}_j \eta \qquad (\text{For } j = 1, \ \dots, \ n_\xi + n_g) \tag{3.13b}$$

then the state-space equations for this column-dependent formulation are given by

$$
s\begin{Bmatrix}\tilde{\boldsymbol{\xi}}\\ s\tilde{\boldsymbol{\xi}}\\ \mathbf{X}_a\end{Bmatrix} = \left[\begin{array}{c|c|c} \mathbf{I} & 0 & 0 \\ \hline 0 & \mathbf{M}-q(\bar{\mathbf{A}}_2)_\xi & 0 \\ \hline 0 & 0 & \mathbf{I}\end{array}\right]^{-1} \left[\begin{array}{c|c|c} 0 & I & 0 \\ \hline -[\mathbf{K}-q(\bar{\mathbf{A}}_0)_\xi] & -[\mathbf{G}-q(\bar{\mathbf{A}}_1)_\xi] & q[\bar{\mathbf{W}}_1 \ \dots \ \bar{\mathbf{W}}_{n_\xi+n_g}] \\ \hline 0 & \bar{\mathbf{V}}_1 \ \dots \ 0 & \bar{\mathbf{H}}_1 \ \dots \ 0 \ 0 \\ \vdots & \vdots \ \ddots \ \vdots & \vdots \ \ddots \ \vdots \ \vdots \\ \vdots & 0 \ \dots \ \bar{\mathbf{V}}_{n\xi} & 0 \ \dots \ \bar{\mathbf{H}}_{n\xi} \ 0 \\ 0 & 0 \ \dots \ 0 & 0 \ \dots \ 0 \ \bar{\mathbf{H}}_{n\xi+n_g}\end{array}\right] \begin{Bmatrix}\tilde{\boldsymbol{\xi}}\\ s\tilde{\boldsymbol{\xi}}\\ \mathbf{X}_a\end{Bmatrix}
$$

$$
+ \left[\begin{array}{c|c|c} \mathbf{I} & 0 & 0 \\ \hline 0 & \mathbf{M}-q(\bar{\mathbf{A}}_2)_\xi & 0 \\ \hline 0 & 0 & \mathbf{I}\end{array}\right]^{-1} \left[\begin{array}{c|c|c|c} 0 & \mathbf{I} & 0 & 0 \\ \hline \mathbf{F}_{\mathrm{HM}} & q(\bar{\mathbf{A}}_0)_g & q(\bar{\mathbf{A}}_1)_g & q(\bar{\mathbf{A}}_2)_g \\ \hline 0 & 0 & 0 & 0 \\ \vdots & \vdots & \vdots & \vdots \\ 0 & 0 & \bar{\mathbf{V}}_g & 0\end{array}\right] \begin{Bmatrix}\mathbf{T}_{\mathrm{HM}}\\ \boldsymbol{\alpha}_g\\ s\boldsymbol{\alpha}_g\\ s^2\boldsymbol{\alpha}_g\end{Bmatrix} \tag{3.14}
$$

where, again, $\tilde{\boldsymbol{\xi}}$ is the vector of Laplace transformed generalized coordinates, and the bar over the $\mathbf{W}_j$ and $\mathbf{H}_j$ denotes the corresponding matrices in terms of s; specifically,

$$
[\bar{\mathbf{W}}(s)]_j = \left[\mathbf{W}\left(\frac{c}{2u}s\right)\right]_j
$$

$$
[\bar{\mathbf{H}}(s)]_j = \left[\mathbf{H}\left(\frac{c}{2u}s\right)\right]_j
$$

Since each $\mathbf{H}_j$ is a square matrix of dimension $n_{L_j} \times n_{L_j}$, the number of aerodynamic states for this column-dependent MMP formulation is

$$
n_a = \sum_{j=1}^{n_\xi+n_g} n_{L_j} \tag{3.15}
$$

If each $n_{L_j} = n_L$, then the number of augmenting aerodynamic states for the MMP formulation is $n_g n_L$ larger than the column-independent LS formulation. If $n_{\delta'}$ actuators can be considered irreversible, the number of augmenting aerodynamic states for the MMP formulation is larger than the LS by an amount $(n_{\delta'}+n_g)n_L$. This amount can be sizable. In every case, however, the MMP fits should be as good as or better than the LS for a fixed n_L because the denominator coefficients are optimized on a per column basis in the MMP approach. The power of the MMP formulation for reduction in added aerodynamic states is maximized by allowing both n_{L_j} and $\{b_{\ell_j}\}$ to vary per column.

If the lag coefficients are the same (same values for $\{b_{\ell_j}\}$ and $n_{L_j} = n_L$) for all columns in the MMP formulation, then the column-dependent state-space equations can be modified to have the same aerodynamic dimension as the column-independent LS formulation as follows. Since each $\mathbf{h}_j(p) = \mathbf{h}(p)$, equation (3.12a) can be rewritten as

$$\hat{\mathbf{Q}}(p) = \mathbf{A}_0 + \mathbf{A}_1 p + \mathbf{A}_2 p^2 + [\mathbf{W}_1(p) \quad \dots \quad \mathbf{W}_{n_\xi + n_g}(p)] \begin{bmatrix} \frac{1}{h(p)} & \dots & 0 \\ \vdots & \ddots & \vdots \\ 0 & \dots & \frac{1}{h(p)} \end{bmatrix} p \tag{3.16a}$$

$$= \mathbf{A}_0 + \mathbf{A}_1 p + \mathbf{A}_2 p^2 + \frac{1}{h(p)} [\mathbf{W}_1(p) \quad \dots \quad \mathbf{W}_{n_\xi + n_g}(p)] p \tag{3.16b}$$

where $h(p)$ is of order n_L, and $\mathbf{W}(p)$ is of dimension $n_\xi \times (n_\xi + n_g)$.

Since $[1/h(p)]\mathbf{W}(p)p$ can be expressed in partial fraction form as

$$\frac{1}{h(p)} \mathbf{W}(p) p = \sum_{\ell=1}^{n_L} \mathbf{A}_{\ell+2} \frac{p}{p + b_\ell}$$

equation (3.16b) is equivalent to equation (3.1a); hence, the aerodynamic dimension corresponding to the state-space realization can be reduced as in section 3.1.1 to that of equation (3.6):

$$n_a = n_\xi n_L \tag{3.6}$$

3.3. Minimum-State RFA Formulation

Karpel suggested in reference 8 that in order to find a minimal augmented state vector, the process of finding aerodynamic approximations and then determining the state-space equations be reversed.

He suggested starting with the general form of the state-space equations defined by

$$s \begin{Bmatrix} \tilde{\xi} \\ s\tilde{\xi} \\ \mathbf{X}_a \end{Bmatrix} = \left[\begin{array}{c|c|c} \mathbf{I} & 0 & 0 \\ \hline 0 & \mathbf{M} - q(\bar{\mathbf{A}}_2)_\xi & 0 \\ \hline 0 & 0 & \mathbf{I} \end{array}\right]^{-1} \left[\begin{array}{c|c|c} 0 & \mathbf{I} & 0 \\ \hline -(\mathbf{K} - q(\bar{\mathbf{A}}_0)_\xi) & -(\mathbf{G} - q(\bar{\mathbf{A}}_1)_\xi) & q\bar{\mathbf{D}} \\ \hline 0 & \bar{\mathbf{E}}_\xi & \bar{\mathbf{R}} \end{array}\right] \begin{Bmatrix} \tilde{\xi} \\ s\tilde{\xi} \\ \mathbf{X}_a \end{Bmatrix}$$

$$+ \left[\begin{array}{c|c|c} \mathbf{I} & 0 & 0 \\ \hline 0 & \mathbf{M} - q(\bar{\mathbf{A}}_2)_\xi & 0 \\ \hline 0 & 0 & \mathbf{I} \end{array}\right]^{-1} \left[\begin{array}{c|c|c|c} 0 & \mathbf{I} & 0 & 0 \\ \hline \mathbf{F}_{\mathrm{HM}} & q(\bar{\mathbf{A}}_0)_g & q(\bar{\mathbf{A}}_1)_g & q(\bar{\mathbf{A}}_2)_g \\ \hline 0 & \mathbf{I} & \bar{\mathbf{E}}_g & 0 \end{array}\right] \begin{Bmatrix} \mathbf{T}_{\mathrm{HM}} \\ \alpha_g \\ s\alpha_g \\ s^2\alpha_g \end{Bmatrix} \tag{3.17}$$

where

$$\bar{\mathbf{R}} = \begin{bmatrix} -\bar{b}_1 & \cdots & 0 \\ \vdots & \ddots & \vdots \\ 0 & \cdots & -\bar{b}_N \end{bmatrix} \tag{3.18}$$

is a diagonal matrix of aerodynamic roots $\bar{b}_\ell$ of some order N necessary to accurately represent the aerodynamic forces. This implies that the aerodynamic states can then be expressed as

$$s\mathbf{X}_a = \left[\bar{\mathbf{E}}_\xi \,\middle|\, \bar{\mathbf{E}}_g\right] \boldsymbol{\eta} + \bar{\mathbf{R}}\mathbf{X}_a \tag{3.19}$$

which can be rewritten as

$$\mathbf{X}_a = [s\mathbf{I} - \bar{\mathbf{R}}]^{-1} \left[\bar{\mathbf{E}}_\xi \,\middle|\, \bar{\mathbf{E}}_g\right] \boldsymbol{\eta} \tag{3.20}$$

Since $\mathbf{R}$ is of dimension $N \times N$, the aerodynamic dimension for this minimum-state formulation is

$$n_a = N \tag{3.21}$$

This aerodynamic dimension N is a parameter which must be determined. Karpel (ref. 8) showed that finding a minimal augmenting state vector satisfying equations (3.17)–(3.21) is equivalent to finding matrices $\mathbf{A}_0$, $\mathbf{A}_1$, $\mathbf{A}_2$, $\mathbf{R}$, $\mathbf{D}$, and $\mathbf{E}$ so that the aerodynamic approximations have the form

$$\hat{\mathbf{Q}}(s) = \bar{\mathbf{A}}_0 + \bar{\mathbf{A}}_1 s + \bar{\mathbf{A}}_2 s^2 + \bar{\mathbf{D}}[s\mathbf{I} - \bar{\mathbf{R}}]^{-1}\bar{\mathbf{E}}s \tag{3.22}$$

which can be written in terms of p as

$$\hat{\mathbf{Q}}(p) = \bar{\mathbf{A}}_0 + \bar{\mathbf{A}}_1 \left(\frac{2u}{c}p\right) + \bar{\mathbf{A}}_2 \left(\frac{2u}{c}p\right)^2 + \bar{\mathbf{D}}\left[\left(\frac{2u}{c}p\right)\mathbf{I} - \bar{\mathbf{R}}\right]^{-1} \bar{\mathbf{E}}\left(\frac{2u}{c}p\right) \tag{3.23}$$

so that

$$\hat{\mathbf{Q}}(p) = \mathbf{A}_0 + \mathbf{A}_1 p + \mathbf{A}_2 p^2 + \mathbf{D}[p\mathbf{I} - \mathbf{R}]^{-1}\mathbf{E}p \tag{3.24}$$

where $\mathbf{D}$ is of size $n_\xi \times N$, $\mathbf{R}$ is a diagonal matrix of size N, and $\mathbf{E}$ is of size $N \times (n_\xi + n_g)$. An iteration method is required to determine a converged solution for the matrices $\mathbf{D}$, $\mathbf{E}$, $\mathbf{A}_0$, $\mathbf{A}_1$, and $\mathbf{A}_2$ in equation (3.24). A higher level nonlinear optimization is designed to optimally select the $\mathbf{R}$.

3.4. Comparison of Aerodynamic Dimension

Typically (but not necessarily), for a given level of total approximation error,

$$\max\{n_{L_j}\} \leq \underbrace{N}_{\substack{n_a \\ \text{for MS}}} \leq \underbrace{\sum_{j=1}^{n_\xi + n_g} n_{L_j}}_{\substack{n_a \\ \text{for MMP}}} \leq \underbrace{n_\xi n_L}_{\substack{n_a \\ \text{for LS}}} \tag{3.25}$$

The character of the matrix corresponding to the lag terms and the resulting aerodynamic dimension required for state-space realization are summarized as follows:

Method	Character of lag terms	Aerodynamic dimension
Extended least-squares	Common lag coefficients in denominator of each matrix element	$n_\xi n_L$
Modified matrix-Padé	Different number of and values for lag coefficients in each column of $\mathbf{Q}$	$\sum_{j=1}^{n_\xi+n_g} n_{L_j}$
Minimum-state	Elements of $\bar{\mathbf{D}}\begin{bmatrix} \frac{1}{s+\bar{b}_1} & \cdots & 0 \\ \vdots & \ddots & \vdots \\ 0 & \cdots & \frac{1}{s+\bar{b}_N} \end{bmatrix}\bar{\mathbf{E}}$	N

Thus the MMP formulation gives more flexibility than the LS approach in the choice and number of lag coefficients and allows them to be determined on a per column basis. In the MS approach, the fact that the number of additional states is independent of n_ξ provides the potential for a large reduction in aerodynamic dimension.

4. Extended RFA Formulations

In most of the applications of aerodynamic approximations in the literature, the denominator coefficients b_ℓ in equation (3.1) have been specified a priori over the range of desired frequencies based on engineering judgment. An alternative approach is to optimize these nonlinear parameters to improve the approximations by improving their selection. Optimization of these parameters has been included in the studies by Dunn (refs. 6 and 7), Tiffany and Adams (ref. 9), and Karpel (ref. 8).

In reference 6, the modified matrix-Padé approximation formulation (which differs slightly in form from the MMP formulation included herein) is indirectly constrained to nearly match certain data points by applying frequency-dependent weighting factors to the corresponding terms in the least-squares solution for the linear coefficients. The nonlinear optimization method of feasible directions of reference 22 is employed therein, using an analytical scheme to compute gradients, when determining the nonlinear parameters.

In reference 8, employing the minimum-state formulation, three fixed equality constraints are imposed on all elements of $\mathbf{Q}$. Explicit inclusion of these constraints reduces the number of degrees of freedom in the least-squares solution. A modification of Davidon's variable metric method (refs. 23–24) and finite differences to approximate gradients (ref. 25) are used in determining the elements b_ℓ of matrix $\mathbf{R}$ in equation (3.24).

In reference 9, the authors extended the least-squares approach (referred to as ELS) to include some capabilities which can have advantages over the modified matrix-Padé approach of reference 6 and the minimum-state approach of reference 8. First, the flexibility in selection of the equality constraints of reference 11 was included in order to improve the fit to the tabular aerodynamic force data in critical regions by imposing certain constraints, or to improve the fit overall by relaxing certain constraints. Second, it employed a numerically stable, non-gradient, nonlinear optimizer to determine the b_ℓ in equation (3.1). This algorithm avoids some numerical difficulties which may arise in the optimization process due to numerical computation of gradients and due to nearly linear dependency of active constraints. Side constraints on the b_ℓ could also be imposed to ensure system stability.

In order to comparatively evaluate the three RFA matrix formulations, the MMP and MS formulations are extended in this paper in a fashion similar to the ELS formulation. These extensions include the same flexibility in selecting equality and side constraints

and include the use of the same nonlinear optimizer. The extended formulations are referred to as the extended modified matrix-Padé (EMMP) and the extended minimum-state (EMS) methods.

In this section, the selectable constraint options will be defined; a common measure of performance of the RFA's will be specified; and the algorithms for determining the optimum values of the free parameters will be specified.

For a given aerodynamic dimension, the optimization of the nonlinear parameters for the ELS, the EMMP, and the EMS formulations results in a smaller total approximation error for suitably constrained approximations than for the LS formulation. Alternatively, optimization of the nonlinear parameters can reduce the aerodynamic dimension for a specified level of total approximation error. For ELS and EMMP, the reduction is indirect since the aerodynamic dimension is a function of both n_L and either n_ξ or $n_\xi + n_g$, respectively. The EMS form, however, is structured in such a way that the aerodynamic dimension equals the order of fit, thus allowing for minimization of the aerodynamic dimension directly.

4.1. Unconstrained Linear Optimization

To determine the linear parameters in the RFA's, a measure of error between the approximating curve and the actual tabular data for each aerodynamic force element is used as an objective or cost function. This particular objective function essentially eliminates the necessity of normalizing the original aerodynamic data. While not apparent in the linear optimization, normalization is essential in the nonlinear optimization (described later) in order for the overall objective function, which is the sum of element errors (ε_{ij}), to be insensitive to differences in magnitudes of the aerodynamic force coefficients.

A square error function is defined by

$$\varepsilon_{ij} = \frac{\sum_n |\hat{Q}_{ij}(ik_n) - Q_{ij}(ik_n)|^2}{M_{ij}} \qquad (4.1a)$$

where

$$M_{ij} = \max_n\{1, |Q_{ij}(ik_n)|^2\} \qquad (4.1b)$$

and $\{k_n\}$ is a set of reduced frequencies for which tabular data are available.

Each term in the sum in equation (4.1a) is a measure of relative error if the maximum magnitude of $Q_{ij}(ik_n)$ is greater than 1, but is an absolute error for magnitudes less than 1. This error function essentially normalizes the aerodynamic data prior to the nonlinear optimization.

A rational approximation of the form of equation (2.6) is linear with respect to the coefficients $(A_m)_{ij}$. If the coefficients $(A_m)_{ij}$ are used as design variables for a particular element of $\mathbf{Q}$ and equation (4.1a) satisfies the *minimum condition* that all partials with respect to each design variable be 0, that is,

$$\frac{\partial \varepsilon_{ij}}{\partial (A_m)_{ij}} = 0 \qquad (\text{For } m = 1, \ldots, n_L) \qquad (4.2)$$

then the resulting system of equations is linear and an algebraic solution for the coefficients $(A_m)_{ij}$ is possible. Henceforth, this will be referred to as a linear optimization. Even though the objective function is quadratic, linear algebraic methods may be employed to determine the optimum solution exactly.

4.2. Constrained Linear Optimization

Several types of equality constraints are considered in references 9–11. Those which have been included here are listed in the next section.

4.2.1. Selectable linear equality constraints. The types of linear equality constraints from which selection can be made (refer to appendix A in ref. 11) are

1. To constrain the values of the RFA's at zero frequency to be the same as the values of the tabular data.
2. To constrain the slopes of the approximating functions at $k = 0$ to be specified values or to satisfy a specified relationship
3. To null out specific coefficients in the approximations
4. To constrain the values of the RFA's at specified nonzero frequency, for which tabular data are interpolated if necessary.

Each constraint is imposed on the entire column j of $\mathbf{Q}$ and can be expressed in terms of linear equations involving the design variables $(A_m)_{ij}$ for a specified j as

$$\mathbf{C}_j^{\mathrm{T}}\{A_m\}_{ij} = \mathbf{C}_{ij}^0 \quad (\text{For } i = 1, \ldots, n_\xi) \qquad (4.3)$$

4.2.2. Lagrange formulation. Equality constraints of types 1 and 3 are included explicitly. The Lagrange multiplier formulation for including constraints of types 2 and 4 is employed to redefine the fit error for a given element of the aerodynamic force coefficient matrix as

$$\varepsilon_{ij}^c = \frac{\sum_n |\hat{Q}_{ij}(ik_n) - Q_{ij}(ik_n)|^2}{M_{ij}} + 2\lambda_{ij}^T \left[\mathbf{C}_j^T \{A_m\}_{ij} - \mathbf{C}_{ij}^0\right] \quad (4.4a)$$

$$= \varepsilon_{ij} + 2\lambda_{ij}^T \left[\mathbf{C}_j^T \{A_m\}_{ij} - \mathbf{C}_{ij}^0\right] \quad (4.4b)$$

where M_{ij} is defined by equation (4.1b).

The number of constraint equations n_{cj} varies per column. The corresponding gradient conditions

$$\frac{\partial \varepsilon_{ij}^c}{\partial (A_m)_{ij}} = 0 \qquad (\text{For } m = 0, \ldots, n_L+2 \text{ (or } n_{L_j}+2)) \quad (4.5a)$$

and

$$\frac{\partial \varepsilon_{ij}^c}{\partial (\lambda_m)_{ij}} = 0 \qquad (\text{For } m = 1, \ldots, n_{c_j}) \quad (4.5b)$$

define a system of linear equations whose algebraic solution determines the numerator coefficients $(A_m)_{ij}$ in equations (3.1), (3.11), and (3.24) and is a least-squares error approximation which exactly satisfies the imposed constraints. The $D_{i\ell}$ and E_{ℓ_j} in equation (3.24) are also determined in this process since

$$\left.\begin{aligned} D_{i\ell} &= (A_m)_{ij} \\ E_{\ell_j} &= (A_m)_{ij} \end{aligned}\right\} \quad (\text{For } m = \ell + 2;\ \ell = 1, \ldots, n_L) \quad (4.6)$$

for alternate steps in the iteration process converging to a solution for $\mathbf{D}$ and $\mathbf{E}$ (refer to section 4.3.3).

4.3. Multilevel Optimization: Linear and Nonlinear

Improvements in the approximations can be made by increasing the number of lag terms. As shown in section 3, however, this increase in the order of fit adversely affects aerodynamic dimension and increases the number of equations required to define the aeroelastic system. The fit can also be improved by reducing the frequency range over which the fits are required, but this reduces the range of applicability (or robustness) of the approximation. The additional free parameters in all the approximations, namely the b_ℓ can be optimized to improve the approximations. Historically, these parameters, or their equivalent in the matrix-Padé approximants, have not been included as design variables since the resulting gradient equations, unlike equations (4.5), are not linear. The technique employed herein to optimize these nonlinear parameters is a nongradient method described in appendix A. This nongradient optimizer has been found to be numerically stable and to possess good convergence properties in the applications to which it has been applied (refs. 9 and 21).

The nonlinear parameters are selected via the nonlinear optimization algorithm to reduce the total column approximation error,

$$J_j = \sqrt{\sum_i w_{ij} \varepsilon_{ij}^c} \qquad (\text{For EMMP}) \quad (4.7a)$$

summed over all rows, or the total matrix approximation error,

$$J = \sqrt{\sum_j J_j^2} \qquad (\text{For ELS and EMS}) \quad (4.7b)$$

summed over all columns. The weighting factors w_{ij} are used to force some of the elements to have more priority than others in determining the nonlinear parameters so that the element error ε_{ij}^c might carry more weight in determining the total error J. These weighting factors could be used to normalize the errors instead of using M_{ij}, but it is easier to weight the importance of elements relative to one another if they are already normalized.

The primary reason for the multilevel, nonlinear optimization structure used in all the formulations being compared herein is to keep the aerodynamic dimension as small as possible without adversely affecting the overall system analyses. The next three subsections present outlines of the optimization processes used by each of the extended approaches. The overall optimization methodology for each extended approximation formulation is depicted in figure 3. Differences in the actual approximation formulations result in variations in the optimization process of selected coefficients, but all three use similar techniques. Each requires a multilevel optimization process in the sense that each contains a closed-form linear least-squares solution for the free linear parameters, which is performed inside an iterative search for parameters that enter the problem in a nonlinear fashion. Furthermore, each method requires that the characteristic roots of the system matrix corresponding to the aerodynamic states be stable. This constraint is enforced during optimization of the nonlinear parameters in the aerodynamic model. The choice of method (ELS, EMMP, or EMS) for a particular application depends on aspects such as the goodness of fit required, computer size and time available, and computer costs.

The optimization of the nonlinear parameters has been included in obtaining "best" approximations using each of the extended LS, MMP, and MS formulations of section 3. The order of fit (n_L for ELS; n_{L_j}, $j = 1, \ldots, n_\xi + n_g$, for EMMP; or N for EMS) is initially selected a priori. Best fits are then determined using this number. The order of fit is then increased or decreased based upon the suitability of the current best fits, until more suitable ones are obtained.

The optimization of the linear coefficients can be considered a first level of optimization. Because of the nature of the objective function and the form of the approximating functions, the ε_{ij}^c can be optimized with respect to the linear coefficients in closed form, eliminating the need for iterative solutions typical in nonlinear optimization. The optimization of the nonlinear parameters may be considered a second level of optimization. It is necessarily an iterative method which employs an algorithm to optimally select the nonlinear parameters. Each selection of nonlinear parameters requires one linear optimization for ELS and EMMP, and more for EMS, to be performed to determine the optimum linear coefficients corresponding to the particular selection of nonlinear coefficients.

Figure 3(a) summarizes the overall optimization processes for the ELS approach, which is column-independent; figure 3(b) summarizes the EMMP approach, which is column-dependent; and figure 3(c) summarizes the EMS process, which incorporates two linear iteration loops within the nonlinear optimization. Initially, in all three approaches, the form of the RFA to be used, the columns (or column) over which the optimization is to be performed, convergence criteria, etc., are identified. The process is then started by selecting an initial set of lag coefficients $\{b_\ell\}_0$ (or $\{b_{\ell_j}\}_0$) and design weights $\{w_{ij}\}$. The vectors of coefficients $\{A_m\}_{ij}$ which minimize the linear equality-constrained objective functions ε_{ij}^c are then determined for each element in the desired column or columns of the matrix $\mathbf{Q}$. The nonlinear objective function J for the ELS and EMS approaches or J_j for the EMMP approach is evaluated and a new set of values for the design variables is determined by the nonlinear optimizer. The best set of $(A_m)_{ij}$'s are then recomputed using matrix techniques. For the EMS approach, the overall process to determine the b_ℓ is the same as for the ELS approach except for the iteration loop to determine the $\mathbf{D}$ and $\mathbf{E}$ which defines a converged minimum value for J with respect to the current nonlinear parameters.

4.3.1. Extended least-squares (column-independent) optimization process. This section outlines the steps in the overall optimization process for the column-independent ELS approach of reference 8. In step 1, the design variables for the linear and nonlinear optimization are separated by considering as design parameters the nonlinear b_ℓ separately from the linear coefficients $(A_m)_{ij}$ in equation (3.1). Figure 3(a) is the flow diagram of the optimization procedure for this ELS approach.

Step 1: For a specified set $\{b_\ell : b_\ell > 0\}$, *perform linear optimization.*

Step 1a:

Determine all the $(A_m)_{ij}$ and λ_{ij}, for each Q_{ij}, which minimize each constrained least-squares error and satisfy specified constraints:

$$\varepsilon_{ij}^c = \frac{\sum_n |\hat{Q}_{ij}(ik_n) - Q_{ij}(ik_n)|^2}{M_{ij}} + 2\lambda_{ij}^T \left[\mathbf{C}_j^T \{A_m\}_{ij} - \mathbf{C}_{ij}^0\right]$$

where

$$M_{ij} = \max_n \{1, |Q_{ij}(ik_n)|^2\}$$

$$\hat{Q}_{ij}(p) = (A_0)_{ij} + (A_1)_{ij} p + (A_2)_{ij} p^2 + \sum_{\ell=1}^{n_L} (A_{\ell+2})_{ij} \frac{p}{p + b_\ell}$$

Step 1b:

Calculate the total objective function

$$J = \sqrt{\sum_j \sum_i w_{ij} \varepsilon_{ij}^c} \tag{4.8}$$

Step 2: Select new set $\{b_{\ell_j} : b_\ell > 0\}$ *using the nonlinear optimizer.*

Repeat steps 1 and 2 until an optimum solution for J is reached.

4.3.2. Extended modified matrix-Pade (column-dependent) optimization process. This section outlines the steps in the overall optimization process for the column-dependent EMMP approach. Figure 3(b) depicts the optimization procedure for this EMMP approach. The distinguishing difference between this optimization process and the column-independent case of section 4.3.1 is that the b_ℓ are no longer the same for all elements in the aerodynamic force matrix $\mathbf{Q}$. In this column-dependent case, they depend

a given column and are necessarily the same only for the elements of that column, rather than for all the columns. This difference in formulation is accomplished simply by a redefinition of the nonlinear objective function, which is now a column objective function identified as J_j. The optimization is now performed as a sequence of linear problems over a specified column for a fixed set of b_{ℓ_j} which are optimally selected by the nonlinear optimizer.

Step 1: For a specified set n_{L_j} *and a set* $\{b_{\ell_j} : b_{\ell_j} > 0\}$, *perform linear optimization.*

Step 1a:

Determine all the $(A_m)_{ij}$ and λ_{ij}, for each element in column j of Q, which minimize each constrained least-squares error and satisfy specified constraints:

$$\varepsilon_{ij}^c = \frac{\sum_n |\hat{Q}_{ij}(ik_n) - Q_{ij}(ik_n)|^2}{M_{ij}} + 2\lambda_{ij}^T \left[\mathbf{C}_j^T \{A_m\}_{ij} - \mathbf{C}_{ij}^0\right]$$

where

$$M_{ij} = \max_n \{1, |Q_{ij}(ik_n)|^2\}$$

$$\hat{Q}_{ij}(p) = (A_0)_{ij} + (A_1)_{ij} p + (A_2)_{ij} p^2 + \sum_{\ell=1}^{n_{L_j}} (A_{\ell+2})_{ij} \frac{p}{p + b_{\ell_j}}$$

Step 1b:

Calculate the column objective function

$$J_j = \sqrt{\sum_i w_{ij} \varepsilon_{ij}^c}$$

Step 2: Select new set $\{b_{\ell_j} : b_{\ell_j} > 0\}$ *using the nonlinear optimizer.*

Repeat steps 1 and 2 until an optimum solution and n_{L_j} for column j have been found.

Repeat entire process for each column $j = 1, \ldots, n_\xi + n_g$.

4.3.3. Extended minimum-state optimization process. This section outlines the steps in the overall optimization process for the EMS approach (fig. 3(c)). In the minimum-state formulation, the numerator coefficients of the lag terms are the product elements of **D** and **E**, namely,

$$(A_{\ell+2})_{ij} = D_{i\ell} E_{\ell_j} \qquad (\text{For } \ell = 1, \ldots, N) \qquad (4.9)$$

Therefore, there are essentially two sets of linear coefficients in each minimum-state approximation, and the minimum-state optimization is necessarily a three-step process. First, an initial set $\{b_\ell\}_0$ of elements for **R** and design weights $\{w_{ij}\}$ are selected and the matrix **D** is set equal to an initializing matrix whose rank is the minimum of n_L and $n_\xi + n_g$. Step 1a in the optimization process is a linear constrained least-squares optimization which determines the best **E**, given **D**. Using this **E** in step 1b, another linear constrained least-squares optimization is performed to determine $\mathbf{A}_0$, $\mathbf{A}_1$, $\mathbf{A}_2$, and a new **D**. Thus steps 1a and 1b express the separation of the design variables for the two linear steps in the overall process for the minimum-state optimization. Step 1c computes the total approximation error J for the results of steps 1a and 1b. Steps 1a to 1c are repeated until the overall objective function J converges using the current set of b_ℓ or hits an alternative stopping criterion, such as a maximum number of iterations. Step 2 then uses the nonlinear optimizer to select a new set of b_ℓ. The entire process continues until an optimal value for the overall objective function is reached.

Step 1: For a specified set $\{b_\ell : b_\ell > 0\}$, *perform linear optimization.*

Step 1a:

For $j = 1, \ldots, n_\xi + n_g$ (using the initial or previously determined **D**), determine all the $(A_m)_{ij}$, E_{ℓ_j}, and λ_{ij}, which minimize the constrained least-squares error ε_{ij}^c simultaneously, for all $i = 1, \ldots, n_\xi$ where

$$\hat{Q}_{ij}(p) = (A_0)_{ij} + (A_1)_{ij} p + (A_2)_{ij} p^2 \sum_{\ell=1}^{n_L} \left(\frac{D_{i\ell} p}{p + b_\ell}\right) E_{\ell_j} \qquad (4.10a)$$

Step 1b:

For $i = 1, \ldots, n_\xi$ (using previously determined **E**), determine all the $(A_m)_{ij}$, $D_{i\ell}$, and λ_{ij}, which minimize the constrained least-squares error ε_{ij}^c simultaneously, for all $j = 1, \ldots, n_\xi + n_g$ where

$$\hat{Q}_{ij}(p) = (A_0)_{ij} + (A_1)_{ij}p + (A_2)_{ij}p^2 + \sum_{\ell=1}^{n_L} D_{i\ell}\left(\frac{E_{\ell_j}p}{p+b_\ell}\right) \qquad (4.10b)$$

Step 1c:

Compute the total objective function

$$J = \sqrt{\sum_j \sum_i w_{ij}\varepsilon_{ij}^c}$$

Repeat Steps 1a–1c until J converges, using the current $\{b_\ell\}$.

Step 2: Select new set $\{b_\ell : b_\ell > 0\}$ *using the nonlinear optimizer which reduces the total objective function, J.*

Repeat steps 1 and 2 until an optimum solution for J is reached.

Figure 3(c) summarizes the overall process which includes the dual-level linear optimizations for **E**, **D**, and the $\mathbf{A}_m$. The additional shaded area in figure 3(c) indicates the logic required by the minimum-state optimization process.

4.4. Side Constraints for Nonlinear Optimization

Since the b_ℓ (or b_{ℓ_j}) are allowed to vary, it is necessary to impose side constraints on them. These lag coefficients must be greater than 0 in order to ensure system stability as a result of introducing the related aerodynamic states into the state equations. Also, it is frequently desired to restrict the range of variation to that in the neighborhood of the range of frequencies over which tabular data are available; that is,

$$0 \le L_\ell < b_\ell < U_\ell \qquad (\text{For } \ell = 1, \ldots, n_L) \qquad (4.11a)$$

or, for column-dependent optimization

$$0 \le L_{\ell_j} < b_{\ell_j} < U_{\ell_j} \qquad (\text{For } j = 1, \ldots, n_\xi + n_g,\ \ell = 1, \ldots, n_{L_j}) \qquad (4.11b)$$

These side constraints are enforced in one of two ways. The first is by way of an inverse sinusoidal transformation of the design space $[L_\ell, U_\ell]$ defined by equation (4.11a) onto the real line segment $[-1, +1]$ (ref. 26). The relationship between the two line segments is

$$b_\ell = \frac{U_\ell - L_\ell}{2}\sin\left(\frac{\pi}{2}z_\ell\right) + \frac{L_\ell + U_\ell}{2} \qquad (4.12a)$$

where

$$-1 \le z_\ell \le 1 \qquad (4.12b)$$

As can be observed, the constraint boundaries are mapped onto $z = \pm 1$. This transformation ensures that the side constraints are always satisfied. However, the restrictions on the z_ℓ, defined by the inequality (4.12b), are not strictly enforced by the nonlinear optimizer. Consequently, an occasional oscillation problem between successive values of the design parameters arises because of the multivalued characteristic of the transformation. Various methods could be applied to avoid this problem; since it rarely occurs, however, a penalty function formulation of the nonlinear objective function (refs. 13, 14, 27, and 28) is employed to enforce the side constraints when it does.

Two examples of available penalty functions are a wall function and the extended-interior penalty function. By wall, we mean that the function essentially hits a wall when constraints are violated. This technique is implemented by defining the objective function as very large relative to its normal range of values. This has extreme discontinuities which can sometimes cause convergence problems and usually requires that an optimization process start within the feasible design space.

The second type of penalty function, proposed by Haftka and Starnes (ref. 27), is an extended-interior formulation. It places no initial restrictions and does not inject discontinuities into the convergence process. This is normally the preferred type of penalty function if convergence problems do arise from the constraint violations since convergence in this case is smoother. The sinusoidal transformation and both the wall and the extended-interior penalty function approaches to constrain the nonlinear parameters have been used in the optimizations presented here.

5. Numerical Application to the DAST ARW-2

The three formulations described in this paper were all applied to a mathematical model of the DAST (Drones for Aerodynamic and Structural Testing) ARW-2 (Aeroelastic Research Wing Number 2) aircraft. The ARW-2 vehicle was designed to have a maximum gross weight of approximately 2500 lb and a wing with a supercritical airfoil having a span of 18.98 ft, an aspect ratio of 10.3, and a sweep angle of 25° at the quarter-chord. The wing was purposely designed to require flutter suppression, maneuver load alleviation, gust load alleviation, and

static stability augmentation in some regions of its flight envelope.

5.1. Description of Mathematical Model

A modal characterization of the ARW-2 was employed which was obtained from a free-free vibration analysis of the ARW-2. Twelve modes were retained for the symmetric degrees of freedom. These are plunge, pitch, and 10 symmetric elastic modes. Table 1 lists the natural frequencies associated with each of the in-vacuum elastic modes. For the results presented here, seven modes were employed. They were composed of 5 of the original 12 modes (–plunge, pitch, and elastic modes 1, 4, and 6), a rigid control surface rotation mode (stabilizer), and a sinusoidal gust mode. The deleted modes had little effect on flutter or rigid body stability and response characteristics. The actuator driving the control mode was considered reversible.

A doublet lattice method (refs. 17 and 18) that is contained in the ISAC system (ref. 15) was used to obtain tabular values of the generalized aerodynamic force coefficients at a Mach number of 0.86 for the following set of reduced frequencies:

$$\{k_n\} = \{0, 0.005, 0.01, 0.05, 0.1, 0.2, 0.3, 0.4, 0.5, 0.6, 0.8, 1.0\}$$

and $\omega_n = (2u/c)k_n$ where $c = 1.956$ ft and $u = 874.75$ ft/sec for the cases studied. The paneling of the lifting surfaces is shown in figure 4(a). The circles indicate points at which mode shape data are defined.

Frequency responses of pitch due to control surface rotation and c.g. acceleration due to control surface rotation were calculated using ISAC and are presented later in this section to illustrate the accuracy of the modeling. Figure 4(b) depicts the locations of the control surface (stabilizer) and the sensors (pitch-rate gyro and c.g. accelerometer) used in these frequency response analyses.

5.2. Baseline Comparisons

As a way of introducing the effects on the RFA's of (1) the number of lag terms and (2) the presence or absence of constraints, some baseline comparisons are presented using the ELS formulation.

5.2.1. Total approximation errors for unconstrained, unoptimized approximations. The first baseline case uses the ELS form for approximating the unsteady aerodynamic forces; different numbers of lag coefficients are used in the approximation, and no constraints are imposed:

Baseline-1 (B1): No equality constraints imposed, no nonlinear optimization

a. 1 lag coefficient (6 states)
b. 2 lag coefficients (12 states)
c. 3 lag coefficients (18 states)
d. 4 lag coefficients (24 states)

Figure 5(a) shows the approximations with 4, 3, 2, and 1 lag term for a single (typical) aerodynamic element (lift due to the fourth elastic mode) with lag coefficients evenly spread over the reduced-frequency range. The open circles are the actual tabular values, and the solid circles are the corresponding values of the approximation at the same values of frequency. The fits deteriorate with a reduction in the order of fit. Other aerodynamic elements (not shown) indicate a similar trend. For each of these unconstrained cases, the total approximation error J for all aerodynamic elements is shown in figure 6.

5.2.2. Total approximation errors for constrained, unoptimized approximations. The second baseline case again uses the ELS formulation for different numbers of lag coefficients in the approximation, but with the following equality constraints imposed:

1. The steady-state values (at $k = 0$) are constrained to agree for all the coefficients:

$$\hat{Q}_{ij}(0) = Q_{ij}(0) \qquad \begin{matrix}(\text{For } i = 1, \ldots, n_\xi \\ \text{and } j = 1, \ldots, n_\xi + n_g)\end{matrix} \tag{5.1}$$

2. The steady-state slopes (at $k = 0$) are constrained for the force coefficients due to –plunge (mode 1) and pitch (mode 2):

$$\left.\frac{\partial \hat{Q}_{i1}(p)}{\partial p}\right|_{p=0} = \frac{Q_{i2}(0)}{b\theta_n} \qquad (\theta_n = -0.00624865) \tag{5.2}$$

$$\left.\frac{\partial \hat{Q}_{i2}(p)}{\partial p}\right|_{p=0} = \frac{\mathrm{Im}[Q_{i2}(ik_2)]}{k_2} \tag{5.3}$$

where assumptions are that $k_1 = 0$ and k_2 is small.

3. For the aerodynamic force coefficients due to the flexible modes, control mode and gust velocity are all constrained to agree with interpolated tabular data at the reduced frequency ($k_f = 0.127$) near flutter:

$$\hat{Q}_{ij}(ik_f) = Q_{ij}(ik_f) \qquad \begin{matrix}(\text{For } i = 1, \ldots, n_\xi \\ \text{and } j = 3, \ldots, n_\xi + n_g)\end{matrix} \tag{5.4}$$

The rationale for constraint 2 is discussed in reference 10 and for convenience to the reader is included

in appendix B. Thus the second baseline case is as follows:

Baseline-2 (B2): Equality constraints imposed, no nonlinear optimization

a. 1 lag coefficient, constrained (6 states)
b. 2 lag coefficients, constrained (12 states)
c. 3 lag coefficients, constrained (18 states)
d. 4 lag coefficients, constrained (24 states)

Figure 5(b) shows a constrained approximation for the same element of **Q** as shown in figure 5(a), but with constraints described as for equation (B2). In each case the fit at and near $k = 0$ is very good and each of the approximating curves also crosses the interpolated curve at k_f.

5.2.3. Comparison of constrained and unconstrained results. Comparing figure 5(a) with 5(b) shows that there is a significant difference between the unconstrained and constrained fits for higher frequencies, and the fits deteriorate drastically for the constrained cases as the order of fit decreases. Both parts of figure 5 demonstrate that the approximating curve can be improved by increasing the number of b_ℓ. Although not shown, the fit can also be improved by reducing the frequency range over which the fits are required, but this reduces the robustness of the approximation. Reduction in frequency range for a column may be desirable if physical considerations dictate that the mode has negligible effect outside some frequency band. Figure 5 also indicates that the number of lag coefficients used in the approximations can be a critical factor in the analyses for which these approximations are being determined.

Table 2 lists the total approximation error J with respect to the aerodynamic dimension for both baseline cases. The approximation error increases with the imposed constraints by almost a factor of 11 for the 6-state case, and a factor of 1.4 for the 24-state case. Figure 6 is a plot of the data in table 2 and indicates more clearly that optimization of the nonlinear coefficients is indeed desirable, especially when constraints are imposed. It is less necessary as the aerodynamic dimension is increased.

5.3. Optimized Comparisons

The optimizations of the nonlinear coefficients using the three rational function formulations described in this paper were performed with the equality constraints imposed as in the baseline-2 cases, resulting in the following optimized cases to be compared:

ELS: Equality constraints (eqs. (5.1)–(5.4)) imposed

EMMP: Equality constraints imposed, the same order of fit assumed for each column

EMMP/v: Equality constraints imposed, the number of denominator coefficients varied for each column

EMS: Equality constraints imposed

Cases Compared

ELS	EMMP	EMMP/v	EMS
6 states (1 lag)	7 states (1 lag)	7–28 states	4 states (4 lags)
12 states (2 lags)	14 states (2 lags)	(varying number	6 states (6 lags)
18 states (3 lags)	21 states (3 lags)	of lags per	7 states (7 lags)
24 states (4 lags)	28 states (4 lags)	column)	8 states (8 lags)
			9 states (9 lags)
			10 states (10 lags)

5.3.1. Total approximation errors for constrained, optimized approximations. Table 3 and figure 7 compare the three extended approximation methods solely in terms of J defined by equations (4.7), for each of the optimized, constrained cases as a function of the aerodynamic dimension. Typically, when optimizing this error function having weighting factors w_{ij}, one would weight important elements more heavily relative to less important ones and perform the fits only over the frequency range pertinent to the problem being analyzed. The weighting factors in the error function for this example, however, were chosen to be 1.0, and the fits were done over the entire frequency range for all elements.

Note that there are two columns in table 3 and two curves in figure 7 that correspond to the EMMP formulation. For the column and curve labeled "EMMP," each column has the same

number n_{L_j} of lag coefficients b_{ℓ_j}, whereas for the column and curve labeled "EMMP/v," n_{L_j} differs between columns. The EMMP/v case, which employs the full flexibility of the matrix-Padé approximation approach, is superior to the EMMP case where n_{L_j} is the same for all columns. As expected, the ELS method, which is required to have the same b_ℓ for each element, has larger approximation error, although slight in this case, than either of the EMMP approaches for a given aerodynamic dimension, and the EMS approach achieves the lowest error of all for a given aerodynamic dimension. One can see by comparing figure 6 with figure 7 or by looking at table 3 that for each formulation, the total error is improved over the corresponding baseline case. Figure 7 also shows that for each formulation, the errors decrease as the aerodynamic dimension increases, but for sufficiently large aerodynamic dimension, the difference in error between the approaches becomes insignificant. This is especially true of the ELS and EMMP approaches.

Another result, which corroborates findings of reference 7, can be seen by comparing, for each formulation, the aerodynamic dimension required to achieve a given level of error. It is shown in figure 7 and table 3 that the fit errors for the minimum-state formulation for low aerodynamic dimensions are comparable to the fit errors for the EMMP and ELS formulations at significantly higher aerodynamic dimensions. For example, the 7-state EMS error falls right between the 12-state ELS error and the 14-state EMMP error, and the 10-state EMS error is approximately equal to the EMMP/v-17 error and only about 12 percent higher than the 24-state ELS error.

The ranking from left to right of the four curves in order of total error for a given aerodynamic dimension seen in figure 7 will hold in general, but the relative spacing between curves will be problem dependent. In general, the ELS would tend to lie further to the right of the EMMP curves. The total approximation error, however, is only one measure of the goodness of the RFA's. The approximations for individual elements must also be examined. Three of the optimized cases, namely,

ELS with 4 lag coefficients, 24 states (ELS-24)

EMMP with 3 lag coefficients per column, 21 states (EMMP-21)

EMS with 10 lag coefficients and 10 states (EMS-10)

were selected for further comparisons since the EMMP-21 and the EMS-10 have nearly the same total approximation errors, and the ELS-24 has an error which is closest in value to the other two.

Cases where one aerodynamic element is difficult to fit but too important to weigh less than the others can occur. This can complicate the process of obtaining satisfactory RFA's by disproportionally influencing the selection of the nonlinear parameters, and for the minimum-state, even the linear parameters. This is illustrated in the next section.

5.3.2. Comparison of fits for selected GAF elements. Figure 8 shows the lift and pitching moment due to each of the seven modes selected for these studies (–plunge, pitch, three elastic modes, control surface rotation, and sinusoidal gust). In figure 8, the short-dashed lines are interpolated fits through the tabular data, indicated by circles, and represent the "truth model." The other lines are the approximating rational functions, and the solid symbols correspond to the values of the approximating functions at the same frequencies as the tabular data. As can be seen from these samples, some of the elements are much harder to fit than others. Since the selection of the b_ℓ is based on the approximation errors for all elements, the ELS and EMS approaches are more sensitive to the hard-to-fit elements than the EMMP approach. The hard-to-fit elements affect the selection of b_{ℓ_j} only for a particular column in the EMMP approach. The EMS is the most sensitive since the numerator coefficients for the lag terms are coupled to all the columns through the matrices **D** and **E**. The driving element, shown in figure 8(n), for the approximations being compared is the pitching moment due to gust. For the set of constraints selected, the EMS actually gives the best fit for this element in the low frequency range, but in doing so, the fits for the other elements are severely degraded.

Table 4 also demonstrates this phenomenon. By comparing the first three columns showing the column error J_j for each of these three cases (ELS-24, EMMP-21, and EMS-10), it can be seen that the EMS-10 case actually obtains the least error for the gust column (column 7), but it does so at the expense of all the other columns. Results of the EMMP/v-17 case (only one lag coefficient for column 2, two lag coefficients for columns 3, 5, and 6, three lag coefficients for columns 1 and 4, and four lag coefficients for the gust column) are shown in the fourth column of table 4 and in figure 9. Comparing these with the EMMP-21 case with three lags per column shows slightly worse fits for the forces due to pitch and elastic modes 1 and 6 and the control mode, which have fewer lag coefficients, the same for those due to plunge and elastic mode 4, which have the same lag coefficients, but are better for those due to

gust, which has one more lag coefficient. The overall error is improved by 7 percent with a reduction in aerodynamic dimension of 19 percent. This can be explained by the fact that fewer lag coefficients are being used for the easier-to-fit elements in order to reduce the aerodynamic dimension without significantly affecting the total approximation error. The additional lag used for the forces due to gust helps to significantly reduce the error in fit for these with only one additional state. Again, however, the gust column even in these cases (EMMP-21 and EMMP/v-17) is driving the total approximation error. Note also the fits overall for the EMMP/v-17 are about as good as the EMS-10 fits as indicated by the fact that the total errors (2.409 and 2.420, respectively, in table 3) are nearly the same.

By relaxing the constraints on the gust column so that the elements are not constrained to fit at the flutter frequency, the curves for the other elements can be improved considerably. Since the EMS-10 was the most sensitive to this constraint, optimizations were performed for this approach with the flutter constraint removed for the gust column as well as the control column. The results are shown in figure 10. In general, the approximations shown are markedly improved. Removal of the constraint to match generalized aerodynamic forces at the flutter frequency for these two columns is reasonable since the stabilizer will be applied only to control low-frequency rigid body motion; and for points removed from flutter, loads due to gust have most of their power concentrated within the rigid body frequency region. In fact, one could also reduce the frequency range of interest, provided that at least as many equations are retained as there are independent variables. For the higher order EMS cases, however, this reduction in frequency range adversely affects the least-squares linear solution.

5.3.3. Comparison of selected frequency responses. Other measures of goodness of fit, such as frequency responses, may also be used to demonstrate the adequacy of candidate p-plane approximations. To illustrate the effects of the three RFA's on "final answers" (i.e., solutions of the aeroelastic equations of motion), each of the three RFA's were implemented in the aeroelastic equations of motion. Pitch and c.g. acceleration frequency response functions due to control deflection were computed for the following flight condition:

Mach number = 0.86
Velocity, $u = 874.75$ ft/sec
Dynamic pressure, $q = 411.5$ lb/ft^2

Figures 11 and 12 contain these frequency response functions. Figure 11 shows the pitch frequency response function and figure 12 shows the c.g. acceleration response due to control deflection for a selected flight condition. Shown on each figure are a baseline case for which no aerodynamic force approximations using rational functions are employed, ELS-24, which had the least total error of the three p-plane approximation cases, and EMMP-21 and EMS-10, both of which had nearly the same value for the total approximation error. There is good agreement between the frequency responses for all three cases, but the ELS is not the best, contrary to what might be expected.

There may be several solutions for the b_ℓ which will give similar total approximation errors. As implied by the results in figures 11 and 12, it may be desirable to consider other measures of how good the approximations are than just the total approximation error itself. The accuracy of key frequency response functions for various fits is another way to assess the adequacy of candidate p-plane approximations.

In summary, these results illustrate some of the factors that should be considered and indicate that considerable engineering judgment may be required to obtain both sufficiently accurate RFA's and low aerodynamic dimension.

5.4. Hidden Costs and Related Problems

The advantage of optimizing the nonlinear coefficients in each of the formulations presented in order to reduce errors for a specified aerodynamic dimension is clear. The ability to significantly reduce the aerodynamic dimension itself using the formulation of reference 8 is especially promising. However, these advantages do not come without cost. A hidden cost here, of course, is the increased computer cost needed to perform the optimizations. The computer costs in the cases compared here are approximately as follows:

ELS = 20 times baseline cost

EMMP = 80 to 100 times baseline cost

EMMP/v = 700 to 1000 times baseline cost

EMS = 2500 to 3000 times baseline cost

These costs may ultimately be offset because the resulting matrices used later in aeroelastic and aeroservoelastic analyses are smaller.

Another hidden cost, in the minimum-state optimization process, is an increased likelihood of computational limitations associated with the EMS due to

the size of the constrained least-squares linear system of equations to solve. These limitations can cause convergence problems in the dual linear optimization used to calculate the total error, which lead to problems within the nonlinear optimization since the approximation error J has not converged. This did not occur, however, for the cases presented.

The desirability of enforcing constraints is based on the physical aspects of the problem being considered. In most instances, flexibility in selecting constraints results in more realistic models and more reliable analyses. Since the larger costs for the minimum-state formulations are due primarily to the internal iterations in the dual linear optimizations, fixing the constraints for all elements as Karpel (ref. 8) did would reduce some of these costs. He enforced the same three constraints for all columns, and using these constraint equations, he solved for the matrices $\mathbf{A}_0$, $\mathbf{A}_1$, and $\mathbf{A}_2$ explicitly, thereby reducing the number of unknowns in the linear optimization. Use of a similar technique on a per-column basis to include some of the selected equality constraints provides a mechanism to reduce the number of unknowns in the linear optimization while retaining the advantages of being able to select desired constraints.

6. Concluding Remarks

Three currently used formulations (namely, a conventional "least-squares" (LS), a modified matrix-Padé (MMP), and a "minimum-state" (MS)) for approximating unsteady aerodynamic forces in the equations of motion of a flexible aircraft with rational functions in the Laplace domain are reviewed. Optimization schemes have been applied to determine the parameters in each formulation. Furthermore, a number of selectable constraints on the approximating functions have been included. This paper extends the modified matrix-Padé and minimum-state approximation methods to the same level of constraint selection and uses the same nonlinear optimization techniques as the extended least-squares method previously developed by the authors. The three extended methods (ELS, EMMP, and EMS) were applied to an aeroservoelastic research model to provide comparative evaluations. Results from the applications show that the number of aerodynamic states employed in representing the equations of motion in linear time-invariant form can be significantly reduced from the number required by the conventional constrained least-squares approach. In fact, the EMMP approach and the EMS approach resulted, respectively, in 24 percent and 67 percent fewer aerodynamic states than a corresponding baseline constrained least-squares approach having a similar total approximation error in which nonlinear parameters were selected a priori. Increases in computer costs as a result of the optimizations performed for ELS, EMMP, and EMS were approximately 20, 700, and 2500 times the cost of the unoptimized baseline approach. In summary, it has been shown that

1. Optimization of the nonlinear parameters improves the approximations in all three formulations.
2. Use of the full flexibility in the modified matrix-Padé formulation (i.e., variable number of lag terms per column) significantly reduces the aerodynamic dimension of the state-space equations of motion from that required when each column has the same number of lag terms.
3. For similar total approximation errors, the aerodynamic dimension for EMMP is less than that for ELS. However, if control surface actuators can be approximated as irreversible rather than reversible, the aerodynamic dimension for ELS decreases and the difference between the two is less.
4. The minimum-state formulation shows great promise in allowing a significant reduction in the aerodynamic dimension of the state-space equations of motion. The approximation errors for the minimum-state formulation for low aerodynamic dimensions are comparable to those for the other two formulations with higher aerodynamic dimension.

Regardless of the formulation used, to obtain sufficiently accurate rational function approximations with low aerodynamic dimension, optimization has to be coupled with engineering judgment to determine the relative importance of individual aerodynamic elements, critical frequency ranges, and appropriate constraints to impose.

NASA Langley Research Center
Hampton, Virginia 23665-5225
March 10, 1988

Appendix A
Nonlinear, Nongradient Optimizer

A.1. Sequential Simplex

The algorithm used to perform the nonlinear optimization in all the RFA formulations presented in this paper is a sequential simplex (or polytope) method developed by Nelder and Mead (refs. 12–14). It has been used in control system design for flexible aircraft with active controls (refs. 20 and 21), along with gradient methods such as the CONMIN feasible direction method (ref. 22), the Davidon-Fletcher-Powell variable metric (refs. 23 and 24), and the newer Davidon optimally conditioned method (ref. 29).

The nongradient Nelder-Mead sequential simplex algorithm is reliable and efficient. The method is simple to use and robust in its ability to handle the nonlinear optimization problem to which it has been applied. Its adaptive nature in moving away from "high" points requires minimal effort on the part of the user to "fine tune" the problem. It is a more stable and robust algorithm, numerically, than some of the gradient-based algorithms to which it has been compared. Since computation of gradients using finite differencing can be costly in large applications programs for which closed-form gradients are either not available or not practical, this nongradient algorithm has proven to be invaluable. It lacks the initial sensitivities of gradient-based methods. But, the final two low values and the step size between them do provide some measure, although somewhat obscure, of sensitivity at convergence. At this point, the gradient could be computed if desired.

The basic mathematical justification of convergence for this algorithm is based only on the convergence of a monotonically decreasing series. Although its order of convergence depends on the function being optimized, it has been found to converge rapidly in numerical applications.

A.2. Description of Algorithm

Figure 13 depicts the algorithm for a two-dimensional design space. The algorithm starts with a simplex of points in the design space (ΔABC). The objective function is evaluated at each vertex in the simplex and the highest valued point is identified (A). A line of projection through the centroid of the opposite side (namely, the other n vertices) is determined and the objective function is then evaluated at the reflected point (E) on the projection line. Depending on the relative value of the function at this point and the other points in the simplex, a single extension (F), a retention (E), an exterior contraction (H), or an interior contraction point (G) is then identified at which the objective function is evaluated and a new simplex is determined. The actual decision process is detailed in references 12–14, although the code as listed (ref. 13) deviates from the decision process as described in the reference with respect to those steps taken when equalities hold.

Appendix B
Rigid Body Slope Constraint

Linear relationships exist between certain functions of some generalized force elements at steady state ($k = 0$) which can be included as constraints on the rational function approximations; see reference 10. An example is illustrated here for the -plunge and pitch modes. As indicated previously (eq. (2.4)) the generalized forces in the reduced-frequency domain are

$$Q_{ij}(s) = \iint_S \frac{\Delta P_j(x,y,s)}{q} z_i(x,y)\, dS \qquad \text{(B1)}$$

which can also be expressed as

$$Q_{ij}(k) = \int z_i(x,y) \times \left[\int \kappa^{-1}(x,y,x',y',k)\frac{w(x',y',k)}{u}\, dS'\right] dS \qquad \text{(B2)}$$

where κ is an influence function that defines the downwash at (x',y') due to a unit pressure disturbance at (x,y). The deflections (z_z, z_θ) and normalized downwash (w_z, w_θ) for the -plunge and pitch modes oscillating at frequency ω, can be expressed in terms of the mode shapes (z_1, z_2) and their slopes, respectively, as follows:

$$\left.\begin{aligned}
&\text{-plunge (mode 1)}\\
&\qquad z_z = z_1\xi_1 = e^{(i\omega t)} = e^{(iu/b)kt}\\
&\qquad \frac{w_z}{u} = \frac{i\omega}{u}e^{(i\omega t)} = \frac{ik}{b}z_z\\
&\text{pitch (mode 2)}\\
&\qquad z_\theta = z_2\xi_2 = -(x - x_{cg})\theta_n e^{i\omega t}\\
&\qquad\quad = -(x - x_{cg})\theta_n e^{(iu/b)kt}\\
&\qquad \frac{w_\theta}{u} = \frac{i\omega}{u}z_\theta - \theta_n e^{i\omega t}\\
&\qquad\quad = \frac{ik}{b}z_\theta - \theta_n e^{(iu/b)kt}
\end{aligned}\right\} \qquad \text{(B3)}$$

Taking the Fourier transform,

$$\left.\begin{aligned}
z_z(k') &= \delta(k'-k)\\
z_\theta(k') &= -(x - x_{cg})\theta_n\delta(k'-k)\\
\frac{w_z}{u}(k') &= \frac{ik}{b}\delta(k'-k)\\
\frac{w_\theta}{u}(k') &= \frac{ik}{b}z_\theta(k') - \theta_n\delta(k'-k)
\end{aligned}\right\} \qquad \text{(B4)}$$

Substituting these into equation (B2) yields the unsteady aerodynamic forces in the reduced-frequency domain:

$$Q_{i1}(k) = \int z_i(x,y)\left[\int \kappa^{-1}(x,y,x',y',k)\,\frac{ik}{b}\, dS'\right] dS$$
$$= \left(\frac{1}{b}\right)\int z_i\left[\int \kappa^{-1}(x,y,x',y',k)(ik)\, dS'\right] dS$$

Hence,

$$\left.\frac{\partial Q_{i1}(k)}{\partial ik}\right|_{k=0} = \left(\frac{1}{b}\right)\int z_i\left[\int k^{-1}(x,y,x',y',0)\, dS'\right] dS$$

Also,

$$Q_{i2}(k) = \int z_i(x,y) \times \left[\int \kappa^{-1}(x,y,x',y',k)\left(\frac{ik}{b}z_\theta - \theta_n\right) dS'\right] dS$$

Hence,

$$Q_{i2}(0) = -\theta_n\int z_i(x,y)\left[\int \kappa^{-1}(x,y,x',y',0)\, dS'\right] dS$$

Therefore,

$$\left.\frac{\partial Q_{i1}(k)}{\partial ik}\right|_{k=0} = \frac{-1}{b\theta_n}Q_{i2}(0)$$

A similar relationship exists between lateral displacement and sideslip or yaw. Explicit enforcement of these constraints improves the prediction of the low-frequency characteristic roots.

References

1. Sevart, Francis D.: *Development of Active Flutter Suppression Wind Tunnel Testing Technology.* AFFDL-TR-74-126, U.S. Air Force, Jan. 1975. (Available from DTIC as AD B002 840L.)
2. Roger, Kenneth L.: Airplane Math Modeling Methods for Active Control Design. *Structural Aspects of Active Controls*, AGARD-CP-228, Aug. 1977, pp. 4-1–4-11.
3. Vepa, Ranjan: *Finite State Modeling of Aeroelastic Systems.* NASA CR-2779, 1977.
4. Edwards, John William: *Unsteady Aerodynamic Modelling and Active Aeroelastic Control.* SUDAAR 504 (NASA Grant NGL-05-020-007), Dep. of Aeronautics and Astronautics, Stanford Univ., Feb. 1977. (Available as NASA CR-148019.)
5. Abel, Irving: *An Analytical Technique for Predicting the Characteristics of a Flexible Wing Equipped With an Active Flutter-Suppression System and Comparison With Wind-Tunnel Data.* NASA TP-1367, 1979.
6. Dunn, H. J.: *An Analytical Technique for Approximating Unsteady Aerodynamics in the Time Domain.* NASA TP-1738, 1980.
7. Dunn, H. J.: An Assessment of Unsteady Aerodynamics Approximations for Time Domain Analysis. *Proceedings of the Aeroservoelastic Specialists Meeting,* AFWAL-TR-84-3105, Vol. 1, U.S. Air Force, Oct. 1984, pp. 98–115.
8. Karpel, Mordechay: *Design for Active and Passive Flutter Suppression and Gust Alleviation.* NASA CR-3482, 1981.
9. Tiffany, Sherwood H.; and Adams, William M., Jr.: *Fitting Aerodynamic Forces in the Laplace Domain: An Application of a Nonlinear Nongradient Technique to Multilevel Constrained Optimization.* NASA TM-86317, 1984.
10. Boeing Commercial Airplane Co.: *Integrated Application of Active Controls (IAAC) Technology to an Advanced Subsonic Transport Project—Wing Planform Study and Final Configuration Selection, Final Report.* NASA CR-165630, 1981.
11. Adams, William M., Jr.; Tiffany, Sherwood H.; Newsom, Jerry R.; and Peele, Ellwood L.: *STABCAR—A Program for Finding Characteristic Roots of Systems Having Transcendental Stability Matrices.* NASA TP-2165, 1984.
12. Nelder, J. A.; and Mead, R.: A Simplex Method for Function Minimization, *Comput. J.*, vol. 7, no. 4, Jan. 1965, pp. 308–313.
13. Olsson, D. M.: A Sequential Simplex Program for Solving Minimization Problems. *J. Qual. Technol.*, vol. 6, no. 1, Jan. 1974, pp. 53–57.
14. Olsson, Donald M.; and Nelson, Lloyd S.: The Nelder-Mead Simplex Procedure for Function Minimization. *Technometrics,* vol. 17, no. 1, Feb. 1975, pp. 45–51.
15. Peele, Ellwood L.; and Adams, William M., Jr.: *A Digital Program for Calculating the Interaction Between Flexible Structures, Unsteady Aerodynamics and Active Controls.* NASA TM-80040, 1979.
16. Bisplinghoff, Raymond L.; and Ashley, Holt: *Principles of Aeroelasticity.* John Wiley & Sons, Inc., c.1962.
17. Albano, Edward; and Rodden, William P.: A Doublet-Lattice Method for Calculating Lift Distributions on Oscillating Surfaces in Subsonic Flows. *AIAA J.*, vol. 7, no. 2, Feb. 1969, pp. 279–285; Errata, vol. 7, no. 11, Nov. 1969, p. 2192.
18. Giesing, J. P.; Kalman, T. P.; and Rodden, W. P.: *Subsonic Unsteady Aerodynamics for General Configurations. Part I, Volume I—Direct Application of the Nonplanar Doublet-Lattice Method.* AFFDL-TR-71-5, Pt. I, Vol. I, U.S. Air Force, Nov. 1971. (Available from DTIC as AD 891 403L.)
19. Newsom, Jerry R.; Abel, Irving; and Dunn, H. J.: *Application of Two Design Methods for Active Flutter Suppression and Wind-Tunnel Test Results.* NASA TP-1653, 1980.
20. Adams, William M., Jr.; and Tiffany, Sherwood H.: *Control Law Design To Meet Constraints Using SYNPAC—Synthesis Package for Active Controls.* NASA TM-83264, 1982.
21. Adams, William M., Jr.; and Tiffany, Sherwood H.: *Design of a Candidate Flutter Suppression Control Law for DAST ARW-2.* NASA TM-86257, 1984.
22. Vanderplaats, Garret N.: *CONMIN—A FORTRAN Program for Constrained Function Minimization—User's Manual.* NASA TM X-62282, 1973.
23. Davidon, William C.: *Variable Metric Method for Minimization.* ANL-5990 Revis. (Contract W-31-109-eng-38), U.S. Atomic Energy Commission, Nov. 1959.
24. Fletcher, R.; and Powell, M. J. D.: A Rapidly Convergent Descent Method for Minimization. *Comput. J.*, vol. 6, no. 2, July 1963, pp. 163–168.
25. Stewart, G. W., III: A Modification of Davidon's Minimization Method To Accept Difference Approximations of Derivatives. *J. Assoc. Comput. Mach.*, vol. 14, no. 1, Jan. 1967, pp. 72–82.
26. Park, Stephen K.: *A Transformation Method for Constrained-Function Minimization.* NASA TN D-7983, 1975.
27. Haftka, Raphael T.; and Starnes, James H., Jr.: Applications of a Quadratic Extended Interior Penalty Function for Structural Optimization. *AIAA J.*, vol. 14, no. 6, June 1976, pp. 718–724.
28. Fletcher, R.: An Ideal Penalty Function for Constrained Optimization. *J. Inst. Math. & Its Appl.*, vol. 15, no. 3, June 1975, pp. 319–342.
29. Davidon, William C.: Optimally Conditioned Optimization Algorithms Without Line Searches. *Math. Program.*, vol. 9, no. 1, 1975, pp. 1–30.

Symbols

$(A_0)_{ij}$, $(A_1)_{ij}$, ... coefficients used in RFA for an element of matrix $\mathbf{Q}$ (see eq. (2.6))

$\mathbf{A}_0, \mathbf{A}_1, \ldots$ matrix of coefficients used in RFA's for matrix $\mathbf{Q}$ (see eq. (3.1))

$\{A_m\}_{ij}$ column vector of coefficients $A_0, A_1, \ldots$ for the (i,j)th element of $\mathbf{Q}$ (see eq. (4.3))

$b_\ell, b_{\ell j}$ constant coefficient in ℓth denominator of partial fraction expansion of RFA for element $Q_{ij}(p)$, of matrix $\mathbf{Q}(p)$; the partial fraction term in the RFA containing this coefficient is commonly referred to as an "aerodynamic lag" term and the b_ℓ as "aerodynamic lag" coefficients or simply, "lag" coefficients (see eqs. (2.6) and (3.11))

c mean aerodynamic chord; reference length is $c/2$

c.g. center of gravity

$\mathbf{C}_j^T$ matrix multiplier of coefficients used in defining linear equality constraints for jth column of $\mathbf{Q}$ (see eq. (4.3))

$\mathbf{C}_{ij}^0$ matrix of constants used in defining linear equality constraints for column of $\mathbf{Q}$ (see eq. (4.3))

$\mathbf{D}$ pre-multiplier numerator matrix for minimum-state formulation (see eqs. (3.17) and (3.24))

$\mathbf{E}$ post-multiplier numerator matrix for minimum-state formulation (see eqs. (3.17) and (3.24))

$\mathbf{F}$ matrix of generalized aerodynamic forces due to aircraft and control surface motions and due to gusts (see eq. (2.2))

$\mathbf{F}_{\mathrm{HM}}$ $n_\xi \times n_\delta$ matrix of modal coefficients converting hinge-moment outputs to generalized forces (see eq. (2.3))

$\mathbf{G}$ matrix of damping coefficients used in Lagrangian formulation of the equations of motion (see eq. (2.2))

$h_j(p)$ denominator polynomial for jth modified matrix-Padé rational function approximation (see eqs. (3.12))

h_{jm} mth coefficient of $h_j(p)$ (see eqs. (3.13))

$\mathbf{H}_j$ state-space matrix multiplier of states in phase-canonical state-space realization of $h_j(p)$ which defines the corresponding augmenting aerodynamic state vector $\mathbf{X}_{a_j}$ (see eqs. (3.13))

$\mathbf{I}$ identity matrix whose dimension depends on equation in which it resides

i complex variable, $\sqrt{-1}$

J total approximation error in approximations for all elements of $\mathbf{Q}$; specifically, weighted sum of square errors in approximations to elements of $\mathbf{Q}$ as a function of lag coefficients currently being used for approximations (see eq. (4.7b))

J_j total approximation error in approximations for all elements in jth column of $\mathbf{Q}$; specifically, weighted sum of square errors in approximations to elements in jth column of $\mathbf{Q}$ as a function of lag coefficients currently being used for that column (see eq. (4.7a))

k nondimensionalized reduced frequency, $\omega c/2u$

k_f reduced frequency corresponding to flutter

k_n reduced frequency at which generalized forces are computed

$\mathbf{K}$ generalized stiffness matrix used in the Lagrangian formulation of the equations of motion (see eqs. (2.2) and (2.3))

$\mathbf{M}$ generalized mass matrix used in the Lagrangian formulation of the equations of motion (see eqs. (2.2) and (2.3))

M_{ij} factor used to normalize element error for nonlinear optimization (see eq. (4.1b))

N number of lag terms and the aerodynamic dimension in the minimum-state formulation

n_a aerodynamic dimension

n_{cj} number of constraint equations for RFA of elements in jth column of $\mathbf{Q}$ (see eq. (4.5b))

n_g number of gust modes retained in equations of motion

n_L number of lag terms (equivalent to number of partial fractions and the order of the overall denominator polynomial) in least-squares RFA (see eqs. (2.6) and (3.1))

n_{Lj} number of lag terms in matrix-Padé RFA's for jth column of aerodynamic forces (see eq. (3.11))

n_δ number of actuators

$n_{\delta'}$ number of irreversible actuators

n_ξ number of modes retained in the equations of motion to define the motion of the vehicle, including control modes

$n_{\xi'}$ number of modes retained in the equations of motion to define the motion of the vehicle, excluding the control modes corresponding to irreversible actuators

p nondimensionalized Laplace variable, $(c/2u)s$

q dynamic pressure

$\mathbf{Q}$ matrix of generalized force coefficients in Laplace domain (see eq. (2.4))

$\hat{\mathbf{Q}}$ matrix of rational function approximations to elements of $\mathbf{Q}$ (see eq. (2.7))

$\mathbf{R}$ diagonal matrix of denominator coefficients used in the minimum-state formulation of the RFA's (see eqs. (3.17)–(3.24))

s complex Laplace variable

S total lifting surface of the aircraft (see eq. (2.4))

t time variable

$\mathbf{T}_{\mathrm{HM}}$ vector of hinge moments output by the actuator (see eq. (2.3))

u reference velocity

$\mathbf{V}_j$ state-space matrix multiplier of inputs in phase-canonical state-space realization of $h_j(p)$ which defines the corresponding augmenting aerodynamic state vector $\mathbf{X}_{aj}$ (see eqs. (3.13))

w_g, v_g vertical and lateral gust velocities

w_{ij} weight applied to the approximation error for the (i,j)th element of $\mathbf{Q}$ in determining the total error J or column error J_j (see eqs. (4.7))

$\mathbf{W}_j$ matrix of polynomial coefficients as defined by equations (3.12), along with equation (3.14) used in matrix-Padé RFA formulation corresponding to jth column of $\mathbf{Q}$

x x-coordinate in spacial coordinate system

$\mathbf{X}_a$ aerodynamic state vector in augmented LTI state-space equations (see eqs. (3.4), (3.13), and (3.20))

y y-coordinate in spacial coordinate system

$z,\ z(x,y,t)$ z-coordinate in spacial coordinate system representing the deflection at a point (x,y) at a given time t (see eq. (2.1))

$z_i,\ z_i(x,y)$ time independent mode shape component of deflection z (see eq. (2.1))

$\boldsymbol{\alpha}_g$ nondimensional gust velocities, $[w_g/u \quad v_g/u]^T$

$\Delta P_j(x,y,s)$ change in the lifting pressure due to changes in the jth generalized coordinate at a point (x,y) on the lifting surface (see eq. (2.4))

$\varepsilon_{ij}(ik_n)$ approximation error between the tabular value and the approximation value of a generalized force at $p = ik_n$ (see fig. 1)

ε_{ij} unconstrained least-square error in fitting an element Q_{ij} of $\mathbf{Q}$ as given by equation (4.1a)

ε^c_{ij} constrained approximation error (in the Lagrangian formulation of the error) for Q_{ij} of $\mathbf{Q}$ as defined by equation (4.4)

η vector of Laplace transformed time derivatives of generalized coordinates and gust inputs, as defined in equation (3.4)

η'_ℓ vector of inputs in state-space realization of least-squares RFA formulation, as defined in equation (3.4)

λ_{ij}	vector of size n_{cj} of Lagrangian multipliers in the Lagrangian formulation of the constrained objective function for the (i,j)th element of $\mathbf{Q}$ (see eqs. (4.4))
ω	frequency of oscillation
θ_n	normalizing angle in definition of rigid body pitch mode shape (see eq. (5.2) and appendix B)
$\xi_i(t)$	generalized coordinate representing the amplitude of the corresponding ith component mode shape in the total deflection as a function of time (see eq. (2.1))
$\xi, \dot{\xi}, \ddot{\xi}$	vector of generalized coordinates and its first two time derivatives used in Lagrangian formulation of equations of motion (see eq. (2.2))
$\tilde{\xi}(s)$	vector of generalized coordinates in Laplace domain (see eq. (2.3))
$\tilde{\xi}'$	vector of generalized coordinates excluding control deflections corresponding to irreversible actuators

Subscripts:

g	related to gusts
i	ith row of matrix $\mathbf{Q}$
j	jth column of matrix $\mathbf{Q}$
ℓ	ℓth partial fraction in RFA
o	initial value
δ	related to controls
ξ	related to generalized coordinates

Notation:

$[\cdot]^T$	transpose of a matrix $[\cdot]$
$\{\cdot\}$	column vector
$-$	bar over a function or matrix indicates that it corresponds to the dimensional Laplace s, rather than the non-dimensional p

Acronyms:

ELS	extended least-squares
EMMP	extended modified matrix-Padé
EMMP/v	extended modified matrix-Padé with varying number of denominator coefficients per column
EMS	extended minimum-state
GAF	generalized aerodynamic force
ISAC	interaction structures, aerodynamics, and controls
LS	least-squares
LTI	linear time invariant
MMP	modified matrix-Padé
MS	minimum-state
RFA	rational function approximation

Table 1. Natural Frequencies of Free-Free Symmetric Elastic Modes for ARW-2

Elastic mode number	Frequency, Hz
1	7.85
2	14.21
3	21.72
4	30.27
5	33.28
6	41.10
7	47.01
8	63.06
9	67.22
10	78.24

Table 2. Baseline (Unoptimized) Approximation Errors in Aerodynamic Approximations

Aerodynamic dimension	Baseline-1, $J^u(a)$	Baseline-2, $J^c(b)$	J^c/J^u
6	4.75	51.88	10.92
12	3.54	7.36	2.08
18	2.58	5.90	2.29
24	1.87	2.59	1.39

[a]Unconstrained approximation error:

$$J^u = \sqrt{\sum_j \sum_i \left[\sum_n \left| \hat{Q}_{ij}(ik_n) - Q_{ij}(ik_n) \right|^2 \Big/ M_{ij} \right]}$$

[b]Constrained approximation error:

$$J^c = \sqrt{\sum_j \sum_i \left[\sum_n \left| \hat{Q}_{ij}(ik_n) - Q_{ij}(ik_n) \right|^2 \Big/ M_{ij} + 2\lambda_{ij}^T \left[C_j^T \{A_m\}_{ij} - C_{ij}^0 \right] \right]}$$

with constraints given by equations (5.1) (steady state), (5.2) and (5.3) (rigid body slopes), and (5.4) (elastic modes near flutter). Capability for explicit inclusion of constraints was not utilized.

Table 3. Optimized, Constrained Approximation Errors in Aerodynamic Approximations

Aerodynamic dimension	Baseline-2, $J^c(a)$	ELS J^c	EMMP J^c	EMMP/v J^c	EMS J^c
4					9.849
5					
6	51.883	22.57			4.796
7			16.238	16.238	4.425
8				11.620	3.442
9				9.069	2.933
10				5.760	2.420
11				5.056	
12	7.362	4.943		4.545	
13				4.151	
14			4.124	3.738	
15				3.302	
16				2.849	
17				2.409	
18	5.900	3.341		2.142	
19				2.015	
20				1.924	
21			2.589	1.833	
22				1.771	
23				1.642	
24	2.591	2.166		1.573	
25				1.517	
26				1.428	
27				1.397	
28			1.828	1.376	

[a]Constrained approximation error:

$$J^c = \sqrt{\sum_j \sum_i \left[\sum_n \left| \hat{Q}_{ij}(ik_n) - Q_{ij}(ik_n) \right|^2 \Big/ M_{ij} + 2\lambda_{ij}^T \left[C_j^T \{A_m\}_{ij} - C_{ij}^0 \right] \right]}$$

with constraints given by equations (5.1) (steady state), (5.2) and (5.3) (rigid body slopes), and (5.4) (elastic modes near flutter). Capability for explicit inclusion of constraints was not utilized.

Table 4. Column Error

	Column	ELS-24	EMMP-21	EMS-10	EMMP/v-17
-plunge	1	0.727	0.688	0.856	0.688
pitch	2	.385	.328	.415	.879
elastic mode 1	3	.204	.248	.398	.633
elastic mode 4	4	.504	.540	.641	.540
elastic mode 6	5	.348	.233	.399	.643
stabilizer	6	.970	.585	1.300	.932
gust	7	1.630	2.318	1.589	1.601

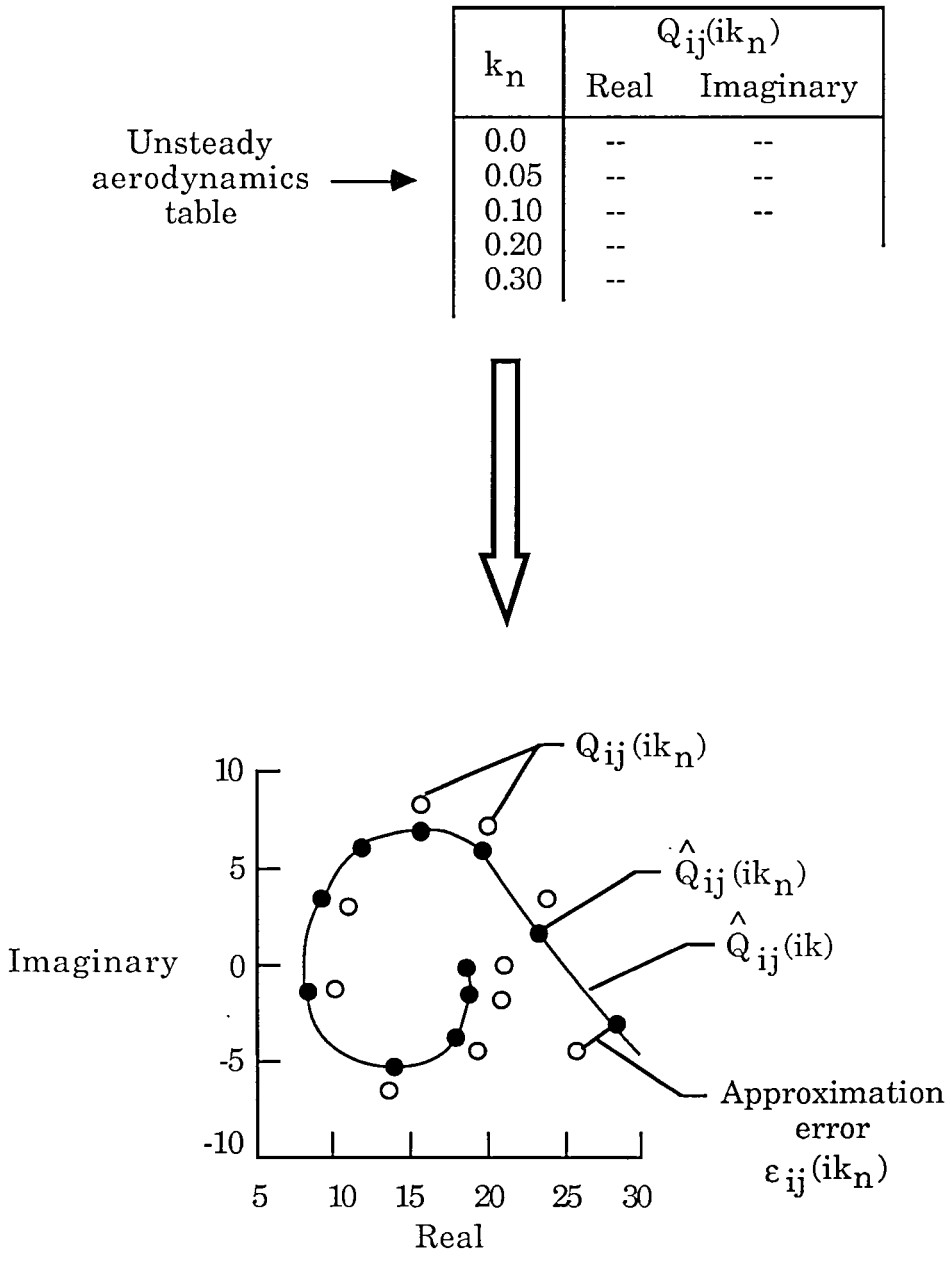

Figure 1. Approximation of aerodynamic data for oscillatory motion by function defined in complex Laplace p-plane.

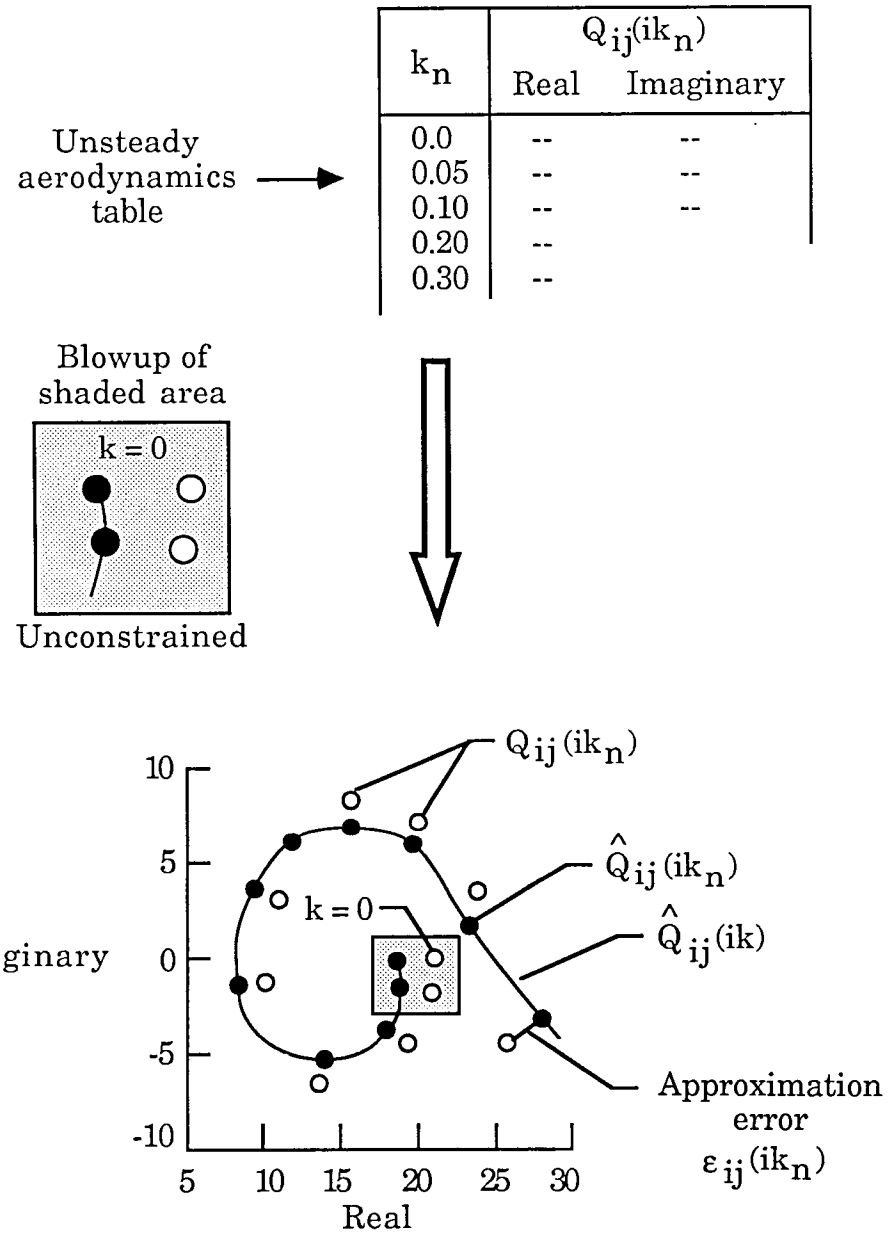

(a) Unconstrained.

Figure 2. Approximation, with and without constraints, of aerodynamic data for oscillatory motion by function defined in complex Laplace p-plane.

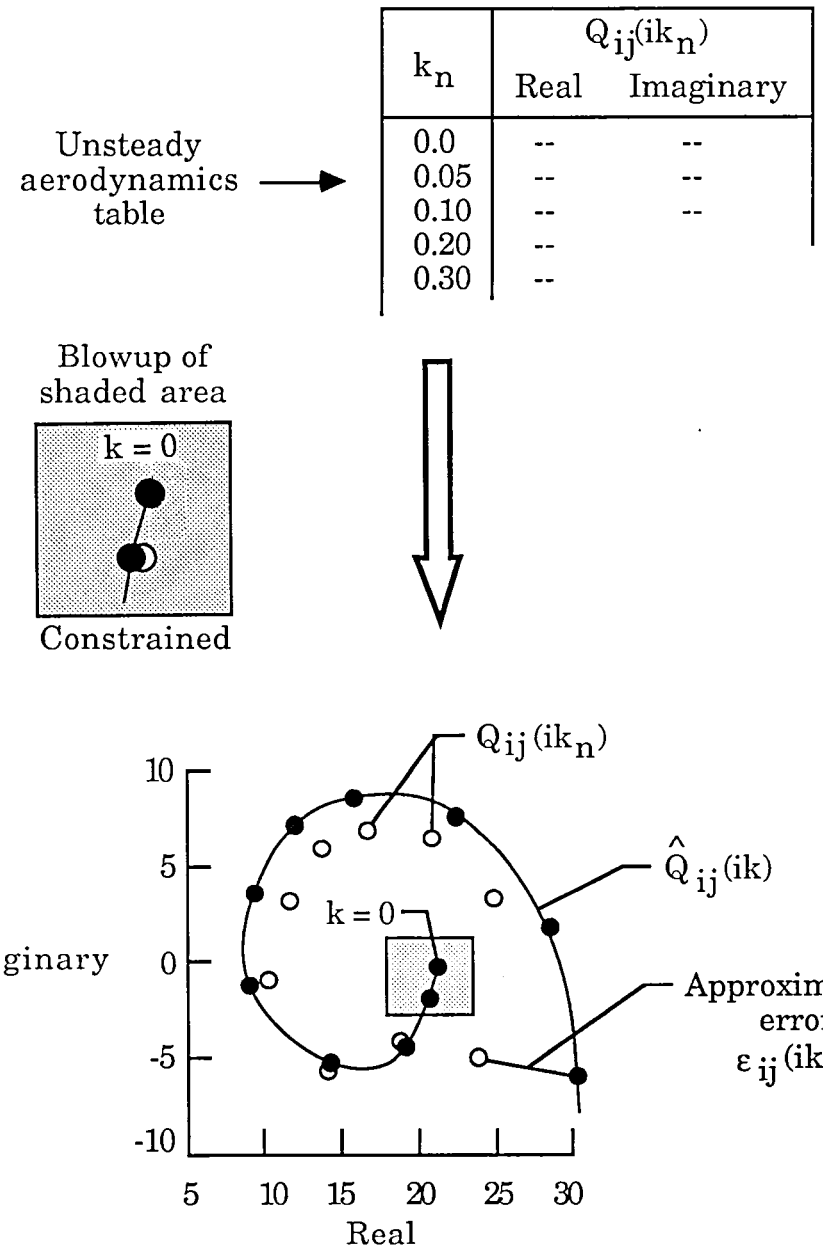

(b) Constrained (at k = 0).

Figure 2. Concluded.

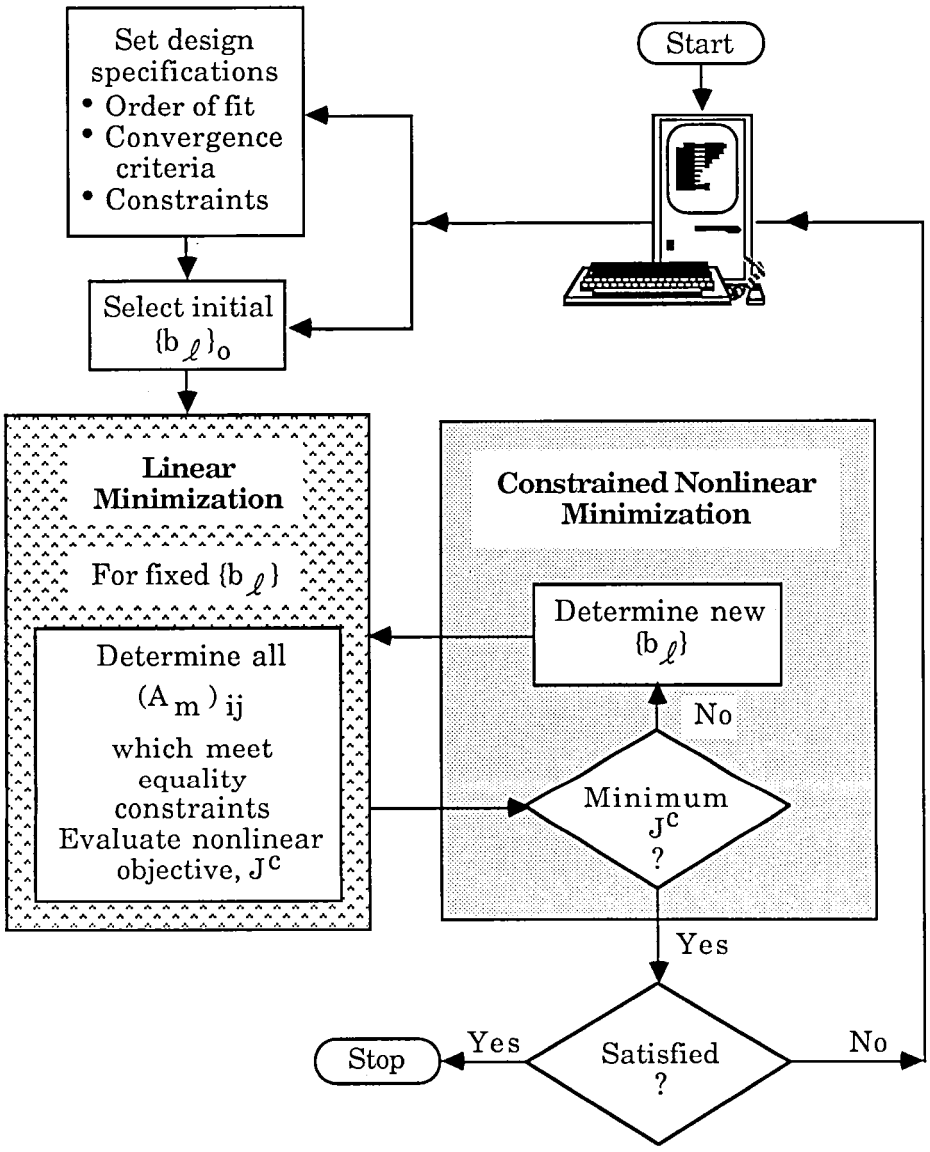

(a) Extended least-squares (ELS), column-independent formulation.

Figure 3. Flow of optimization procedures for extended approximation methods.

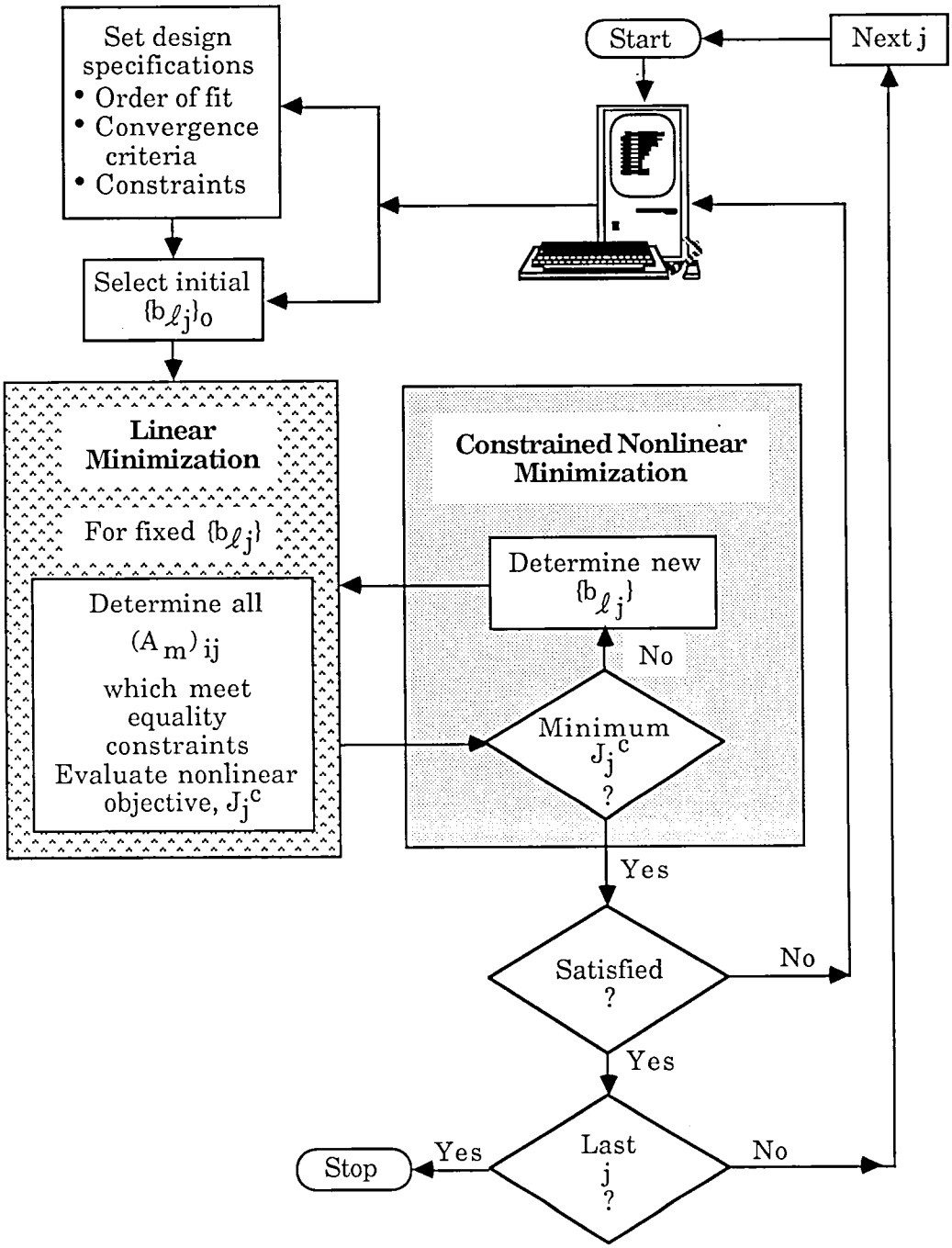

(b) Extended modified matrix-Padé (EMMP), column-dependent formulation.

Figure 3. Continued.

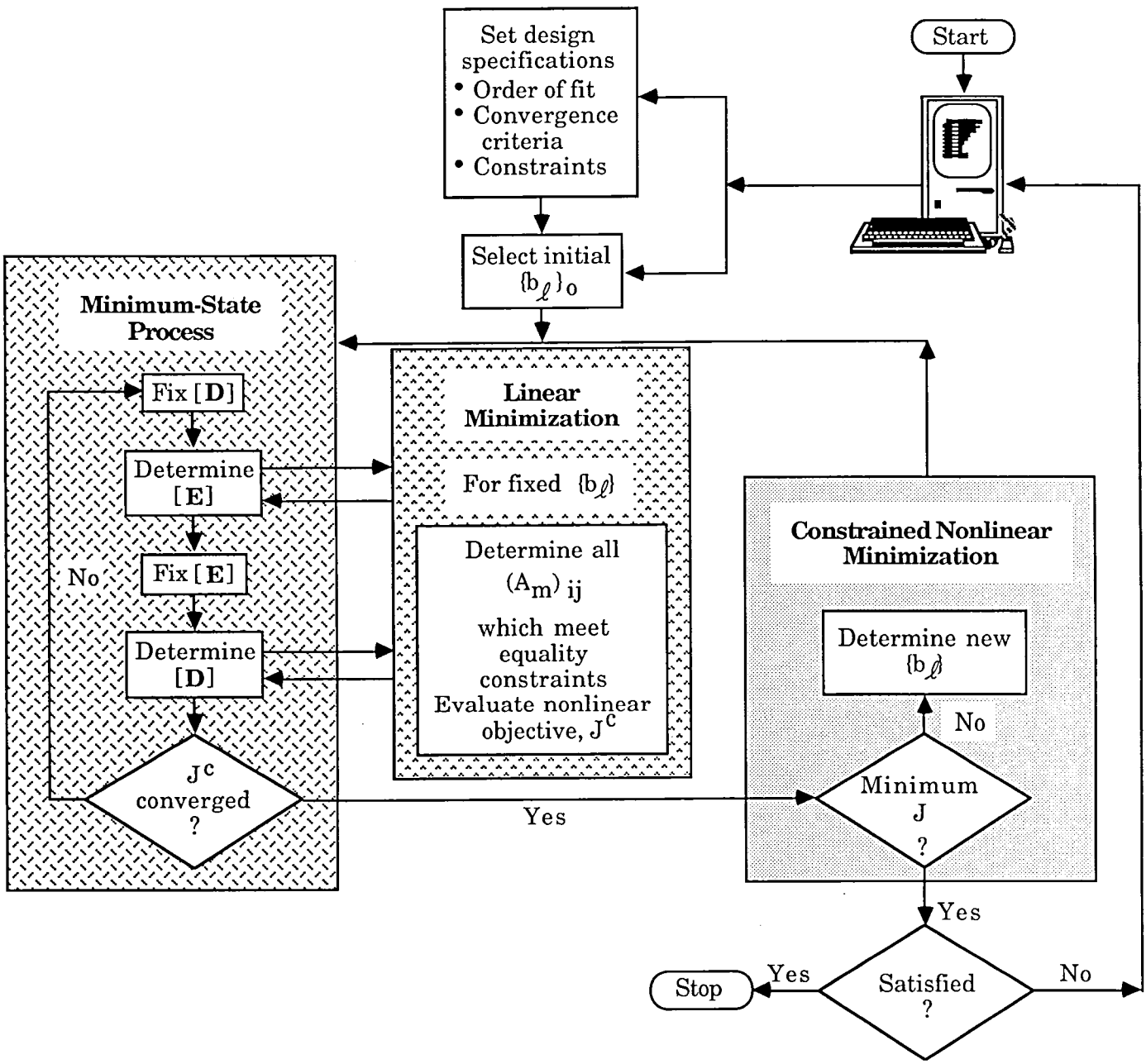

(c) Extended minimum-state (EMS) formulation.

Figure 3. Concluded.

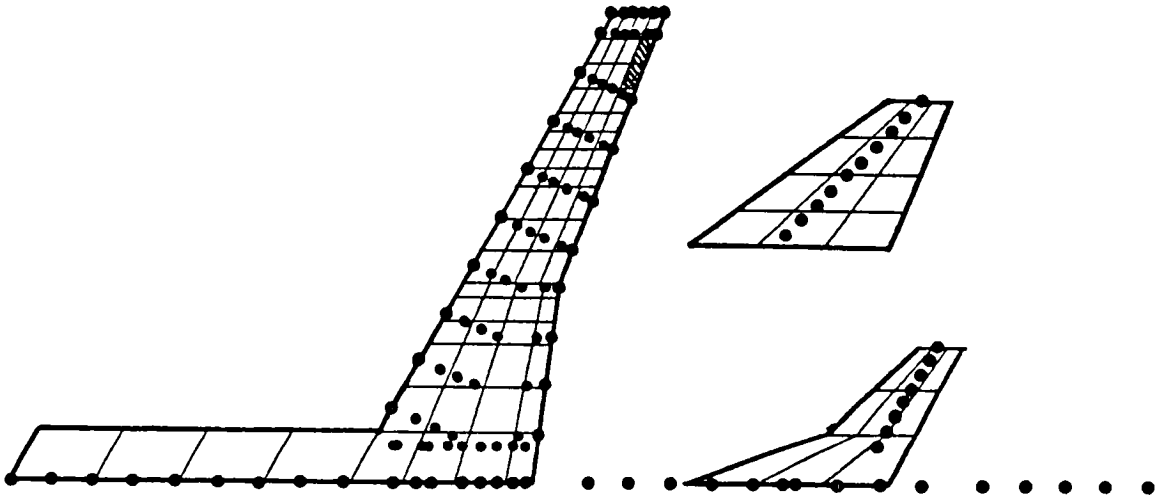

(a) Paneling of lifting surfaces for unsteady generalized aerodynamic force calculations.

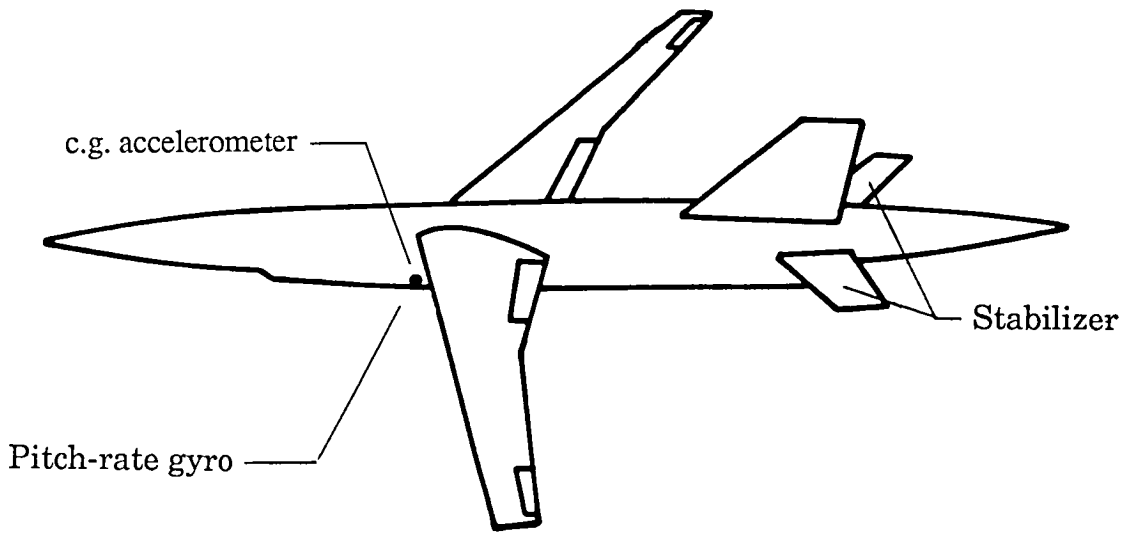

(b) Location of sensors and control.

Figure 4. Aerodynamic paneling and locations of sensors and control for DAST ARW-2 used in frequency response analyses.

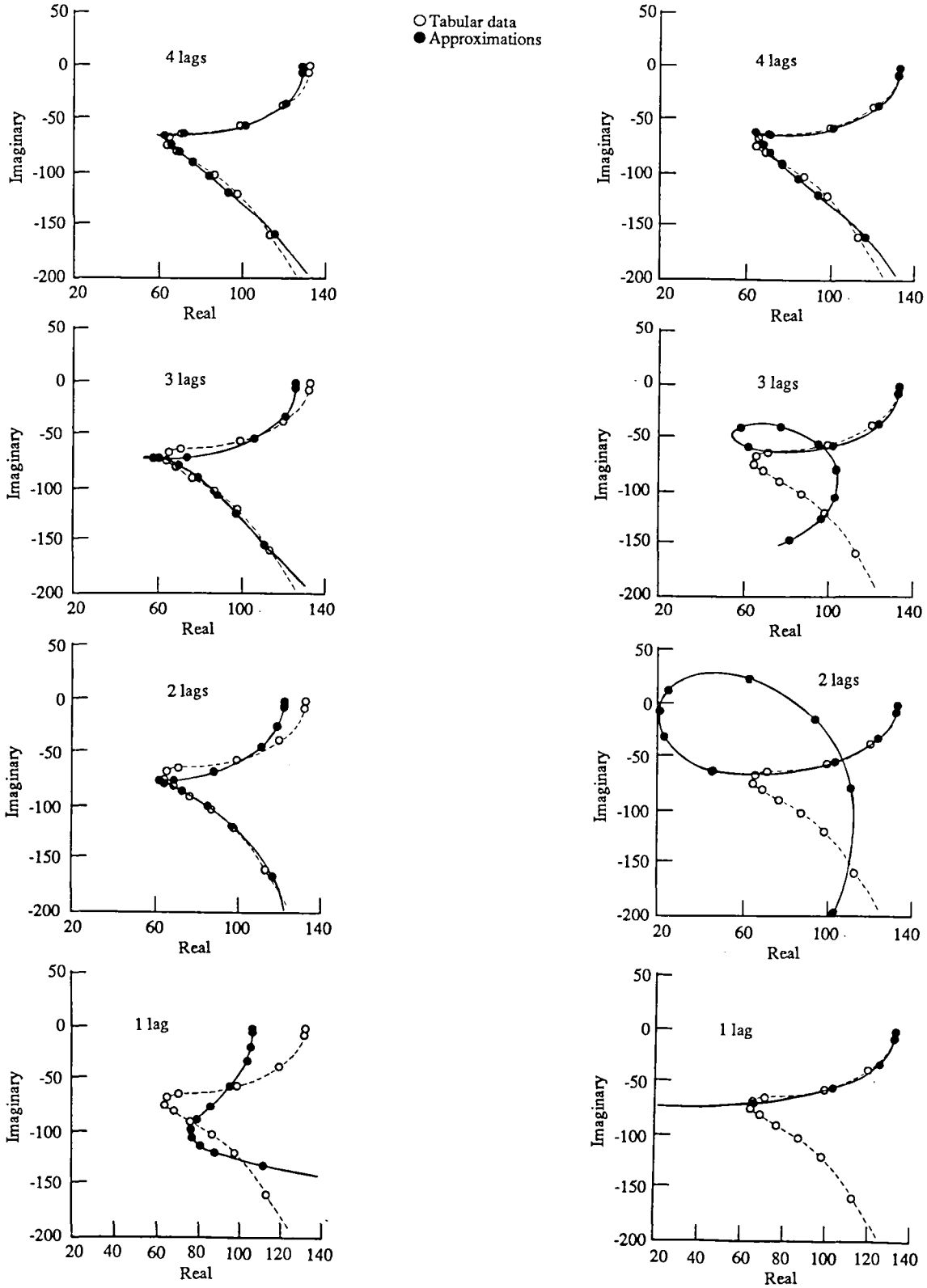

(a) Unconstrained.

(b) Constrained.

Figure 5. Unoptimized (baseline) least-squares approximations for lift due to fourth elastic mode using lag coefficients chosen a priori.

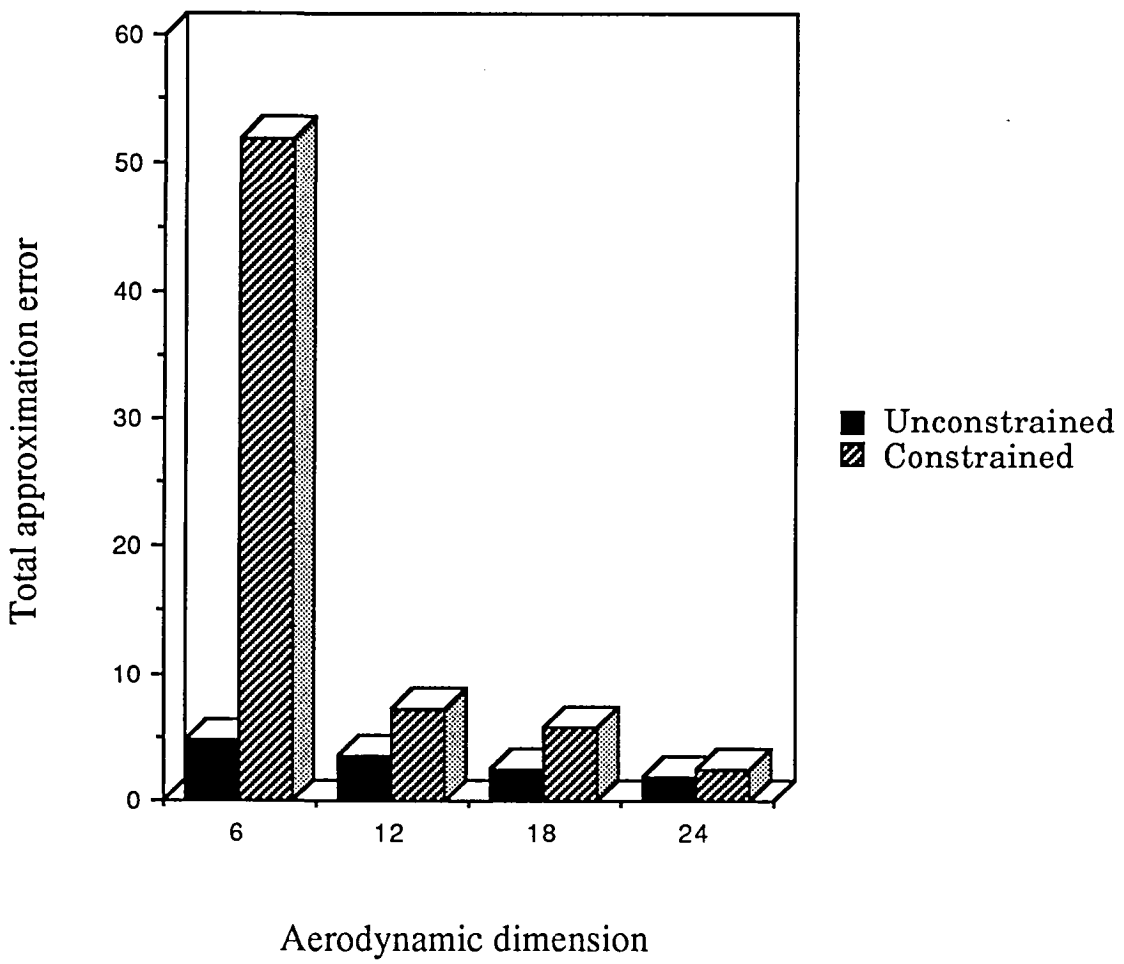

Figure 6. Unoptimized (baseline) least-squares total approximation errors for unconstrained and constrained approximations.

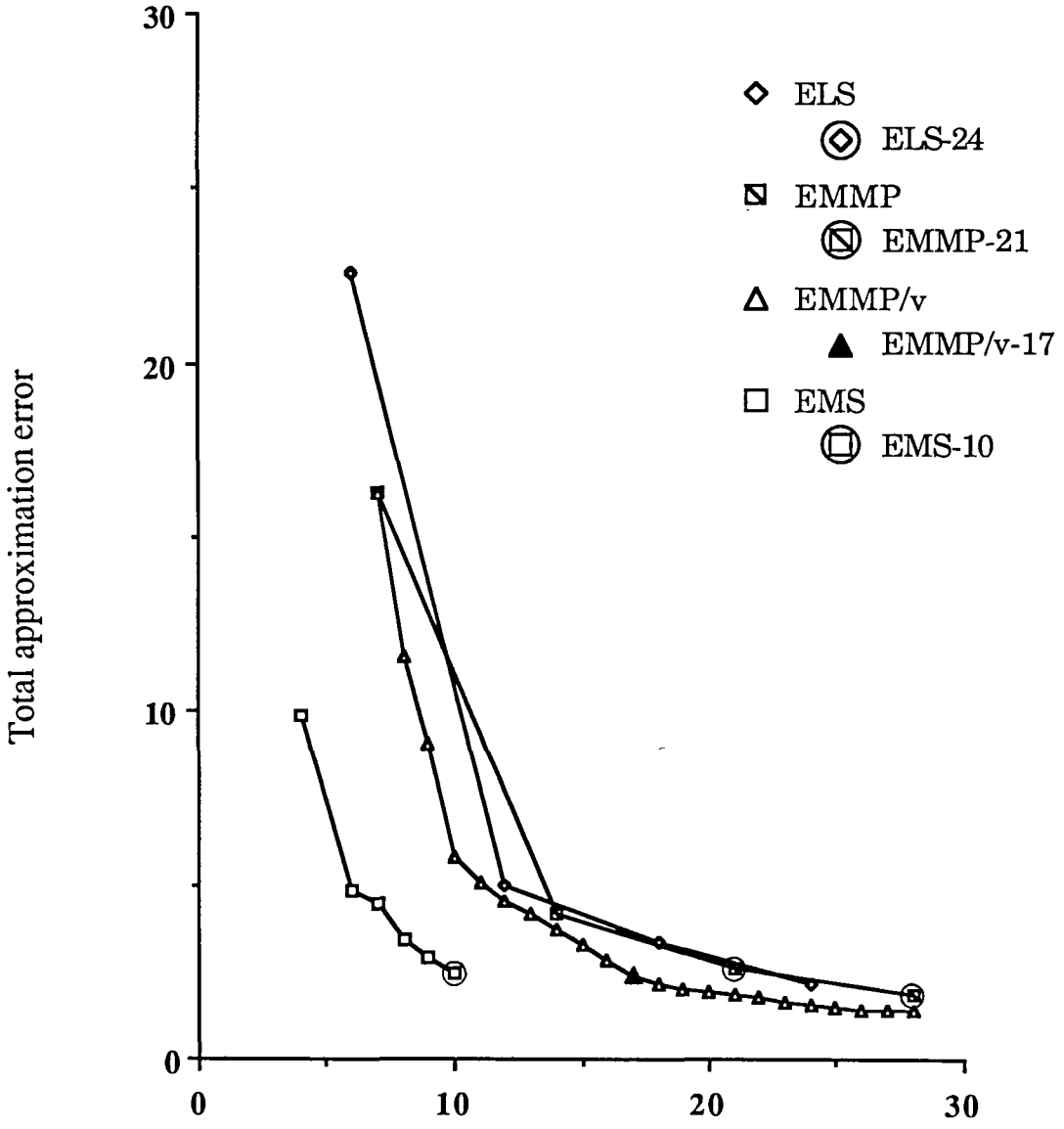

Figure 7. Optimized, constrained total approximation errors in three extended approaches to approximating unsteady aerodynamic forces.

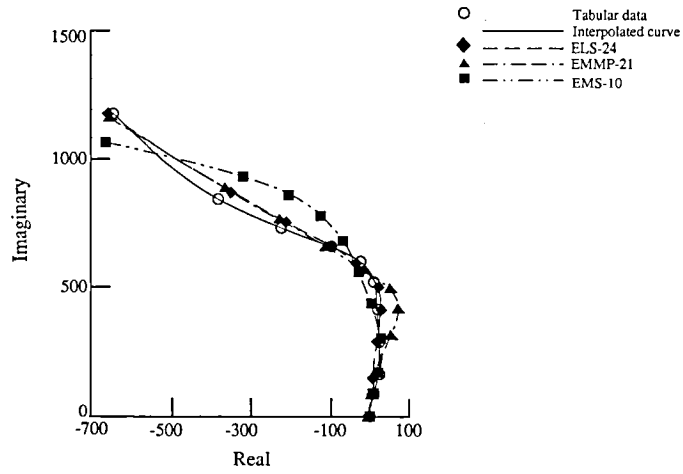

(a) Lift due to plunge.

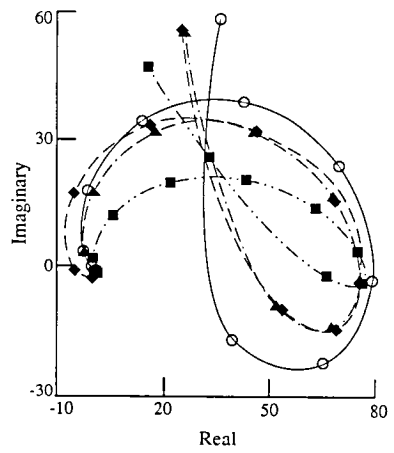

(b) Pitching moment due to plunge.

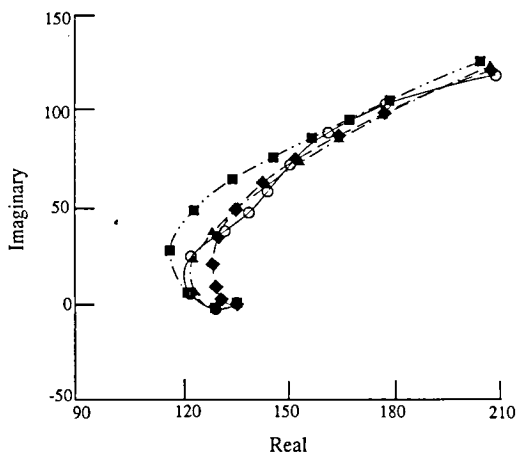

(c) Lift due to pitch.

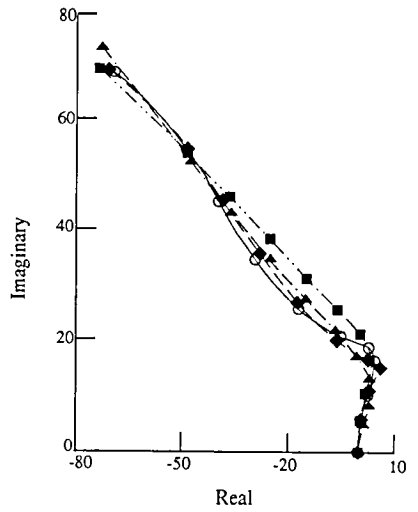

(d) Pitching moment due to pitch.

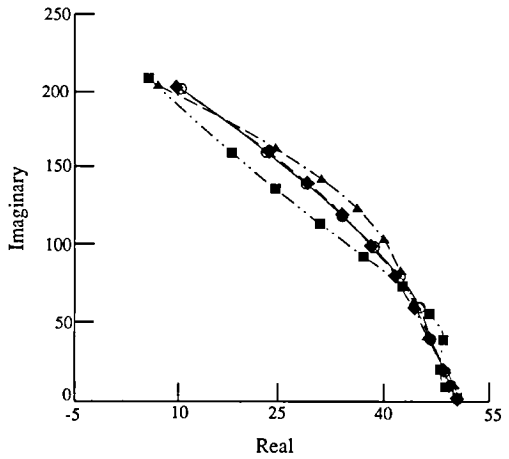

(e) Lift due to elastic mode 1.

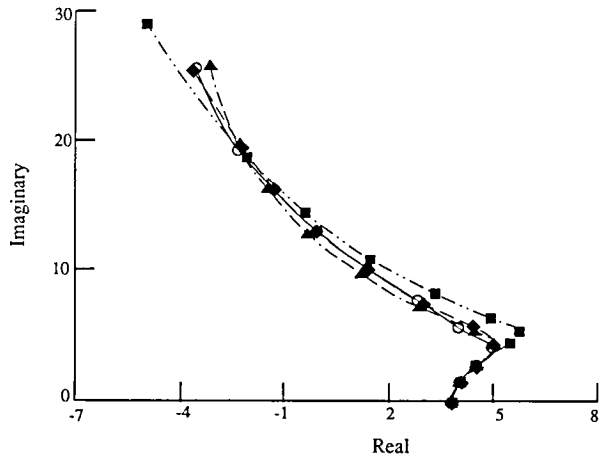

(f) Pitching moment due to elastic mode 1.

Figure 8. RFA plots for selected, optimized ELS, EMMP, and EMS approximations.

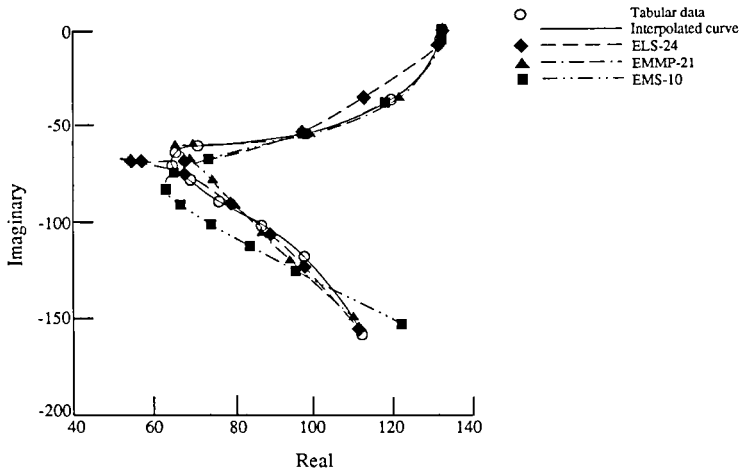

(g) Lift due to elastic mode 4.

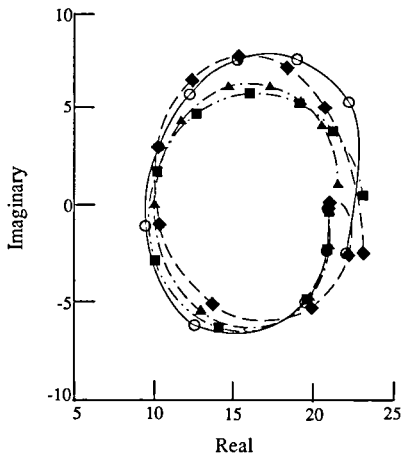

(h) Pitching moment due to elastic mode 4.

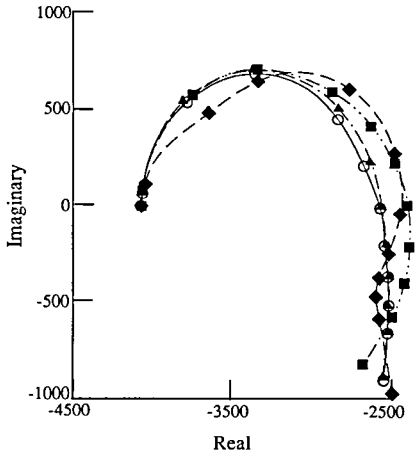

(i) Lift due to elastic mode 6.

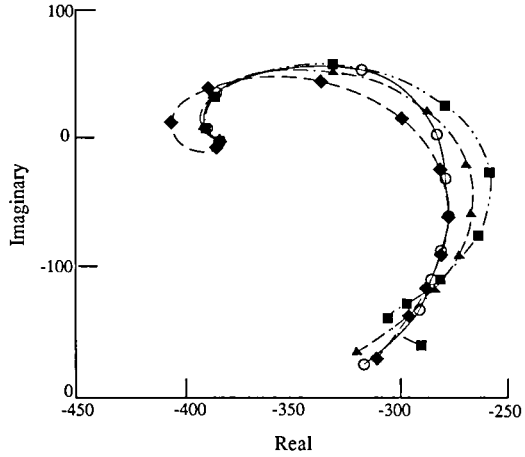

(j) Pitching moment due to elastic mode 6.

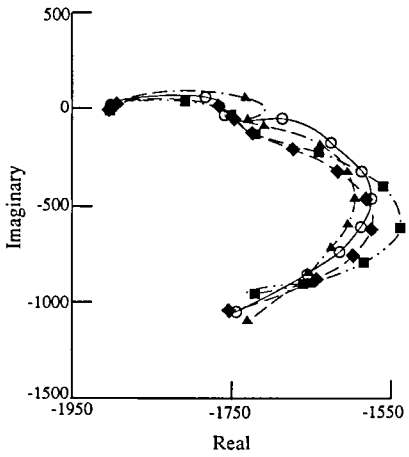

(k) Lift due to control.

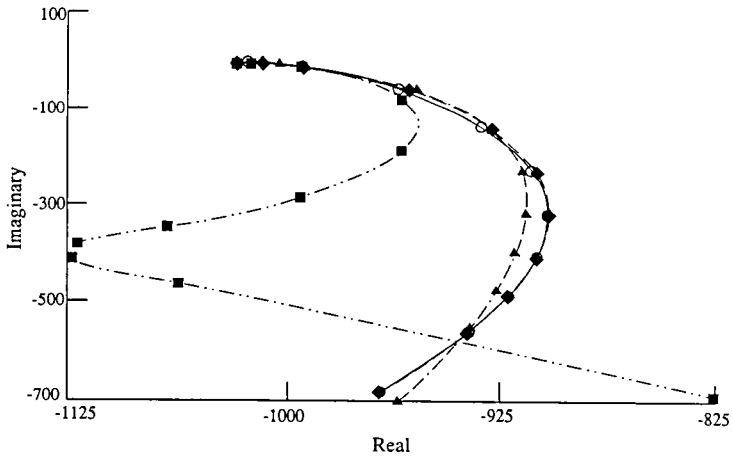

(l) Pitching moment due to control.

Figure 8. Continued.

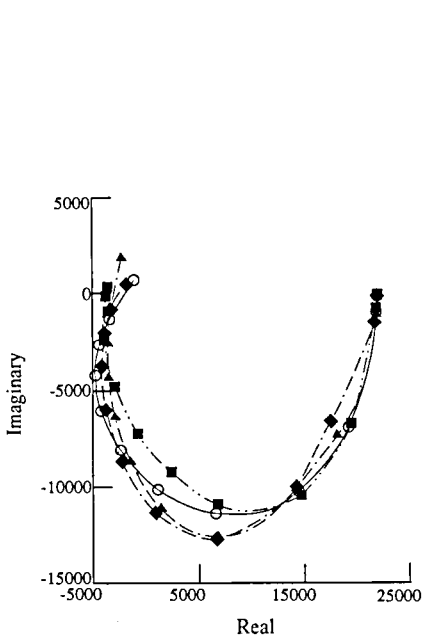

(m) Lift due to gust.

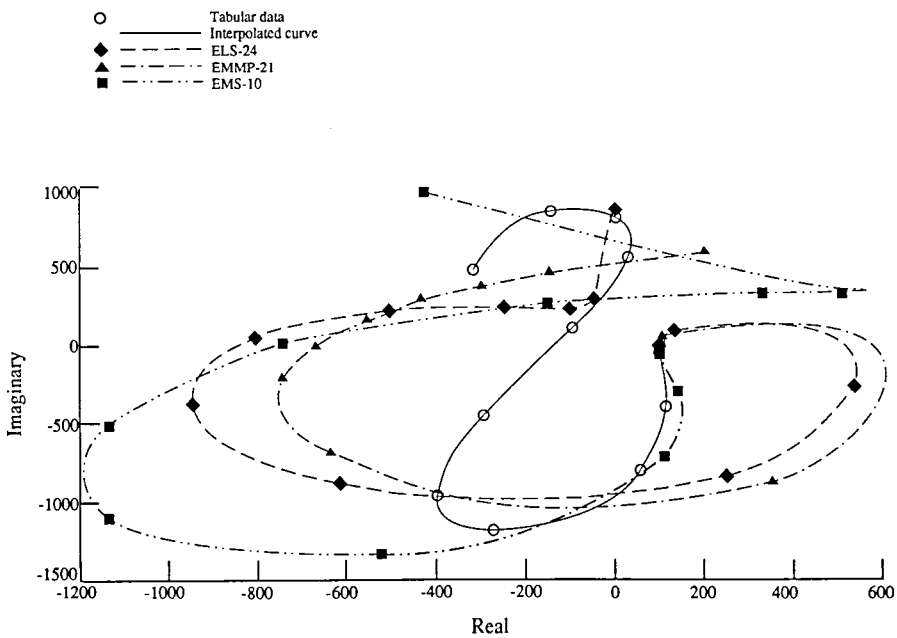

(n) Pitching moment due to gust.

Figure 8. Concluded.

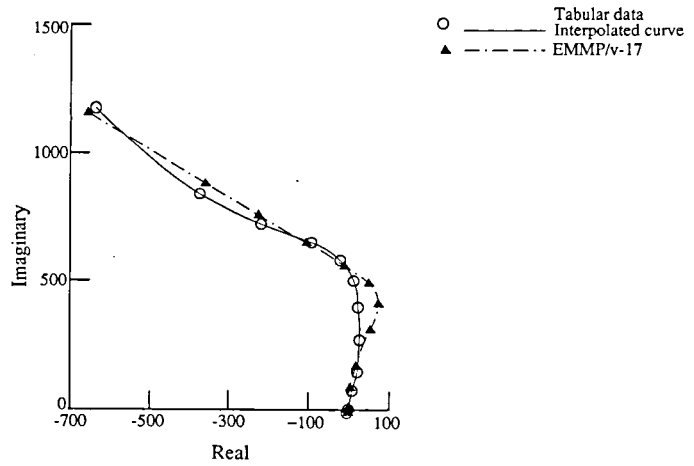

(a) Lift due to plunge.

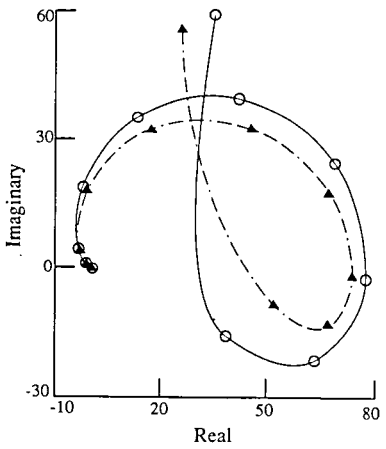

(b) Pitching moment due to plunge.

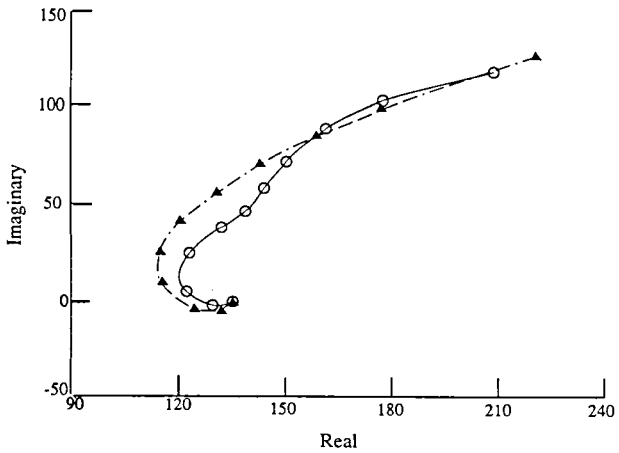

(c) Lift due to pitch.

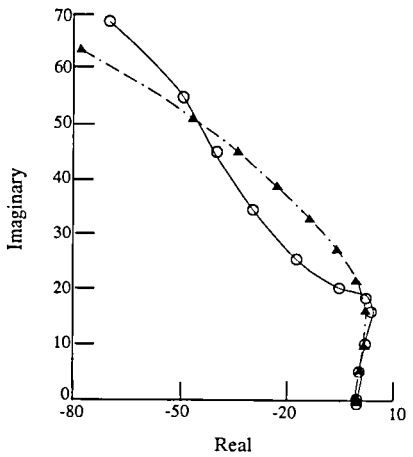

(d) Pitching moment due to pitch.

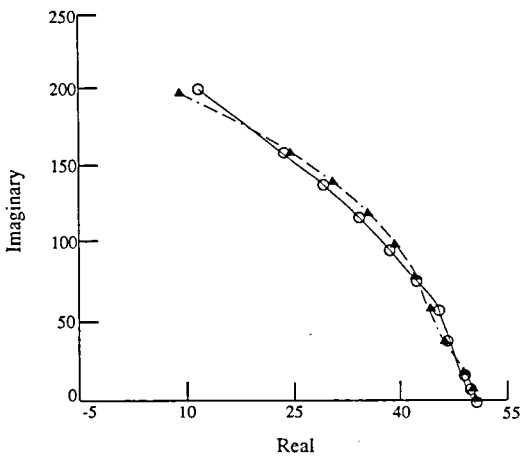

(e) Lift due to elastic mode 1.

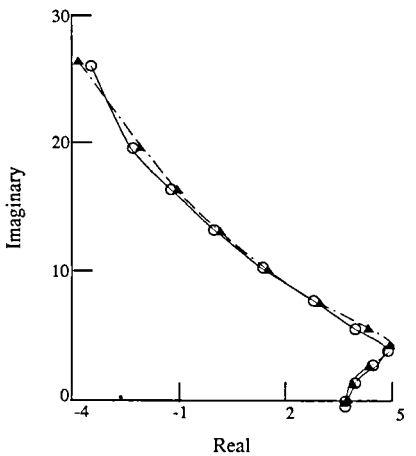

(f) Pitching moment due to elastic mode 1.

Figure 9. RFA plots for selected, optimized EMMP approximations for the 17-state case (EMMP/v-17).

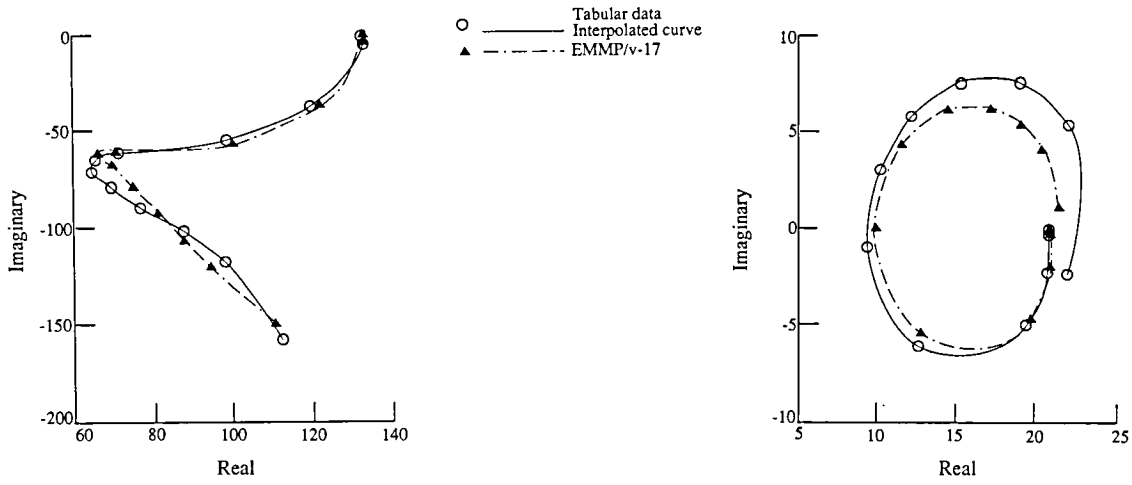

(g) Lift due to elastic mode 4.

(h) Pitching moment due to elastic mode 4.

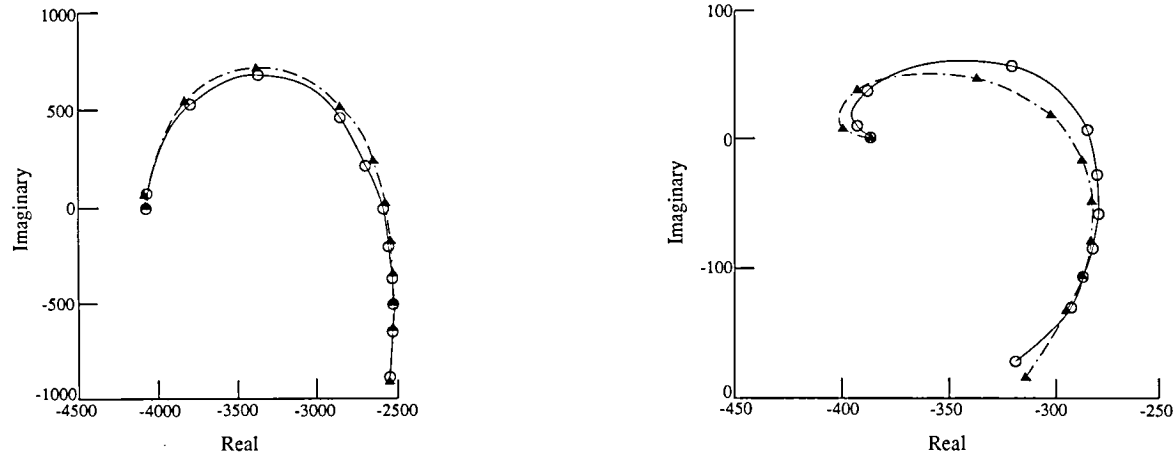

(i) Lift due to elastic mode 6.

(j) Pitching moment due to elastic mode 6.

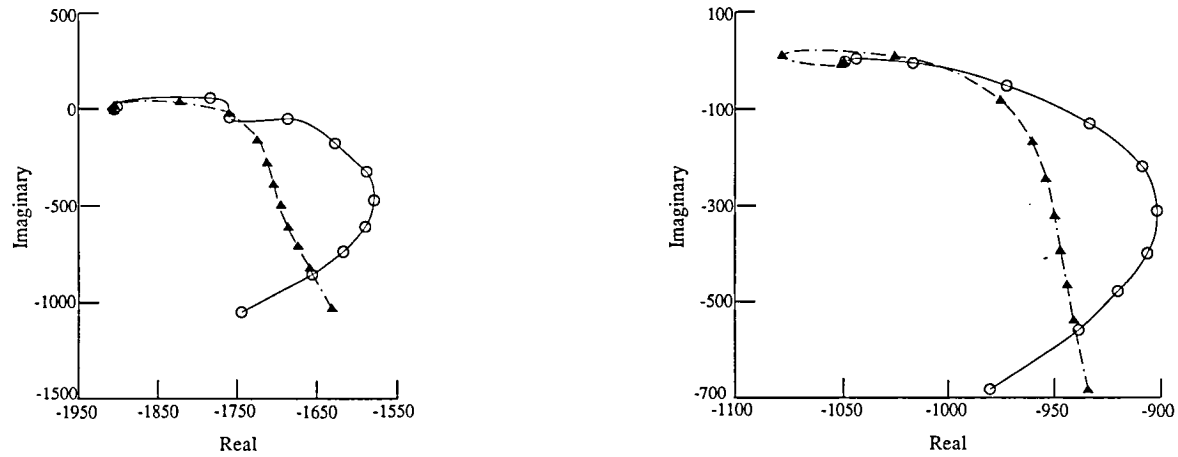

(k) Lift due to control.

(l) Pitching moment due to control.

Figure 9. Continued.

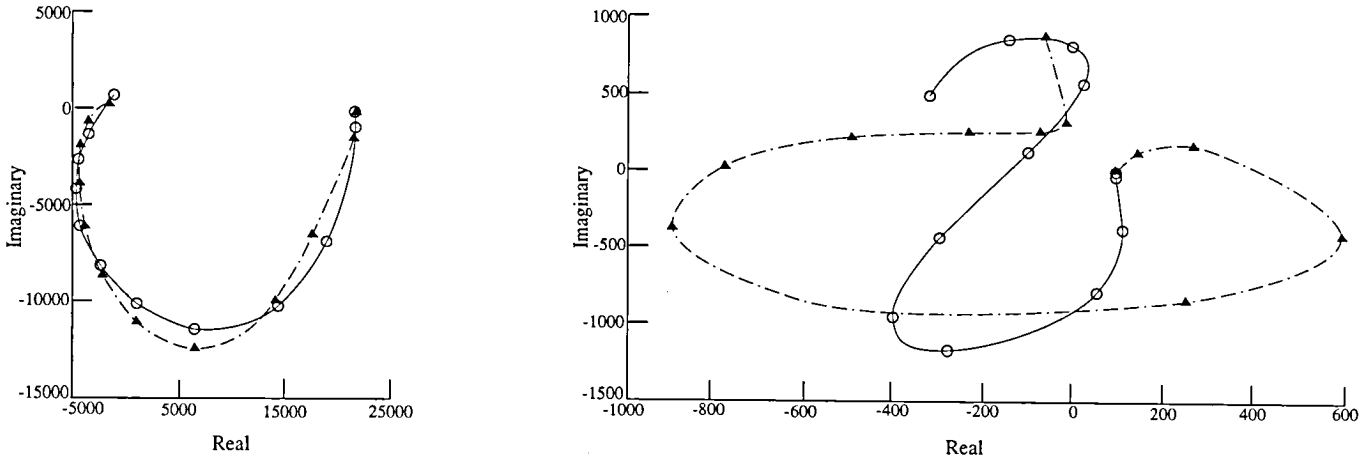

(m) Lift due to gust.

(n) Pitching moment due to gust.

Figure 9. Concluded.

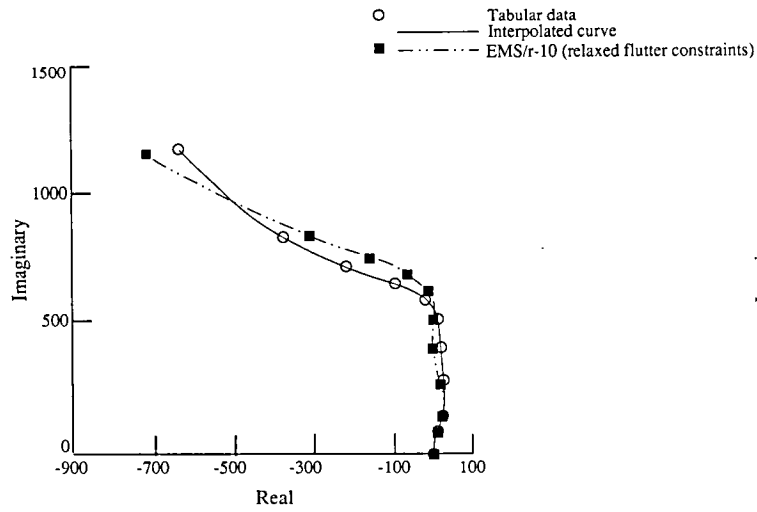

(a) Lift due to plunge.

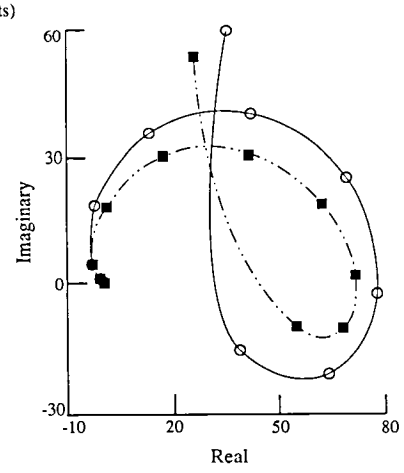

(b) Pitching moment due to plunge.

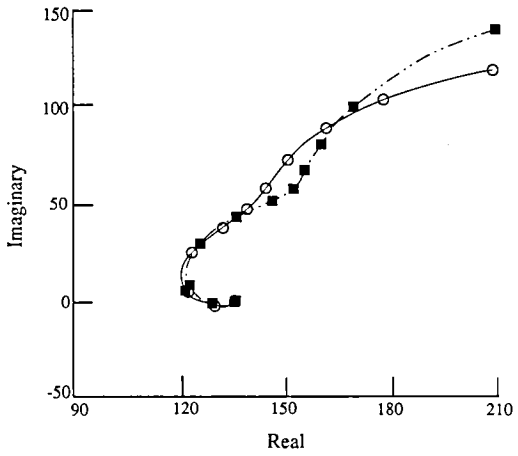

(c) Lift due to pitch.

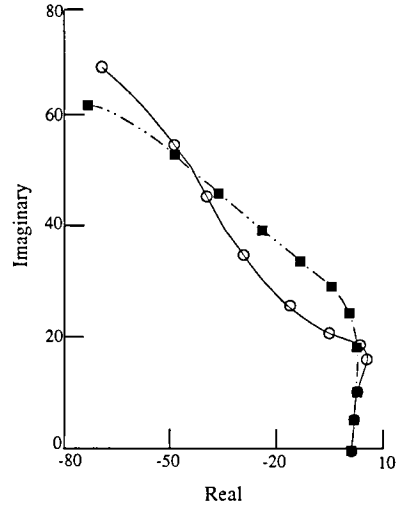

(d) Pitching moment due to pitch.

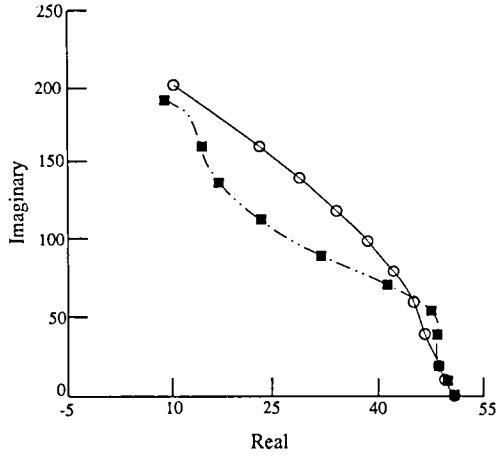

(e) Lift due to elastic mode 1.

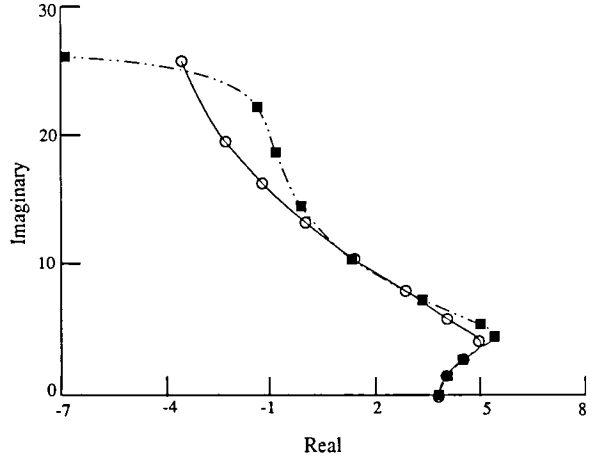

(f) Pitching moment due to elastic mode 1.

Figure 10. RFA plots for selected, optimized EMS approximations for the 10-state case in which flutter frequency constraints are removed for last two modes.

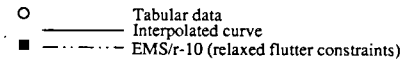

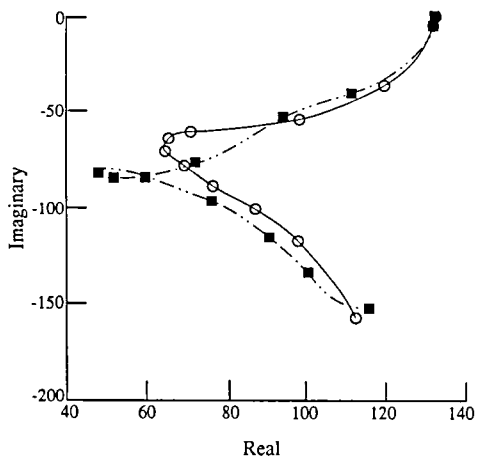

(g) Lift due to elastic mode 4.

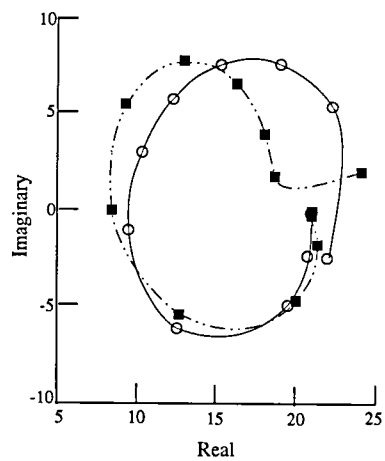

(h) Pitching moment due to elastic mode 4.

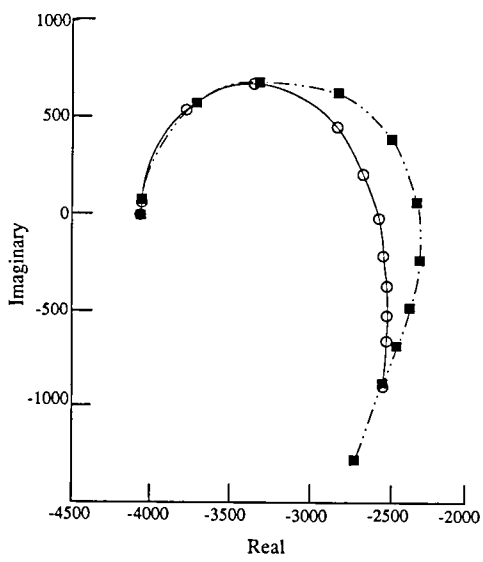

(i) Lift due to elastic mode 6.

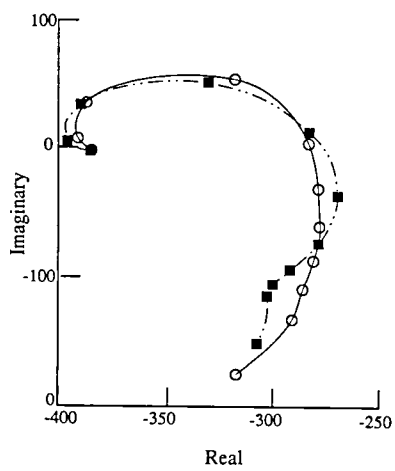

(j) Pitching moment due to elastic mode 6.

Figure 10. Continued.

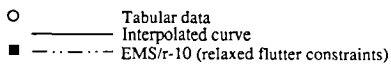

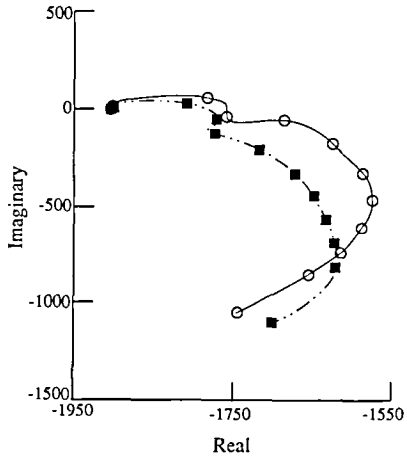

(k) Lift due to control.

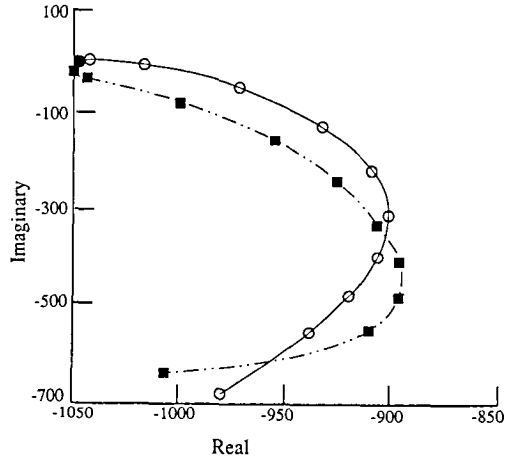

(l) Pitching moment due to control.

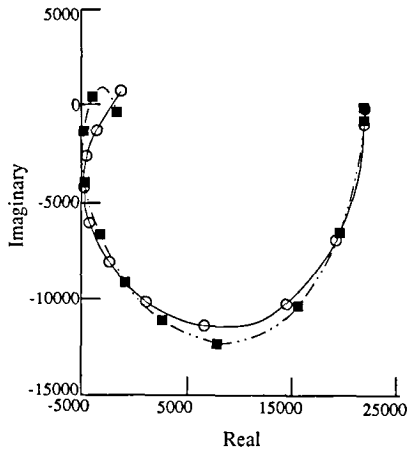

(m) Lift due to gust.

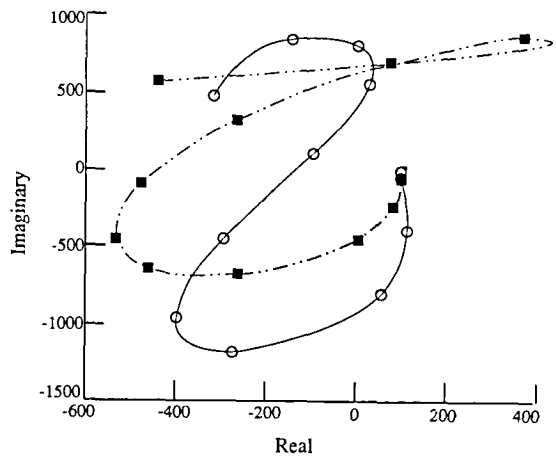

(n) Pitching moment due to gust.

Figure 10. Concluded.

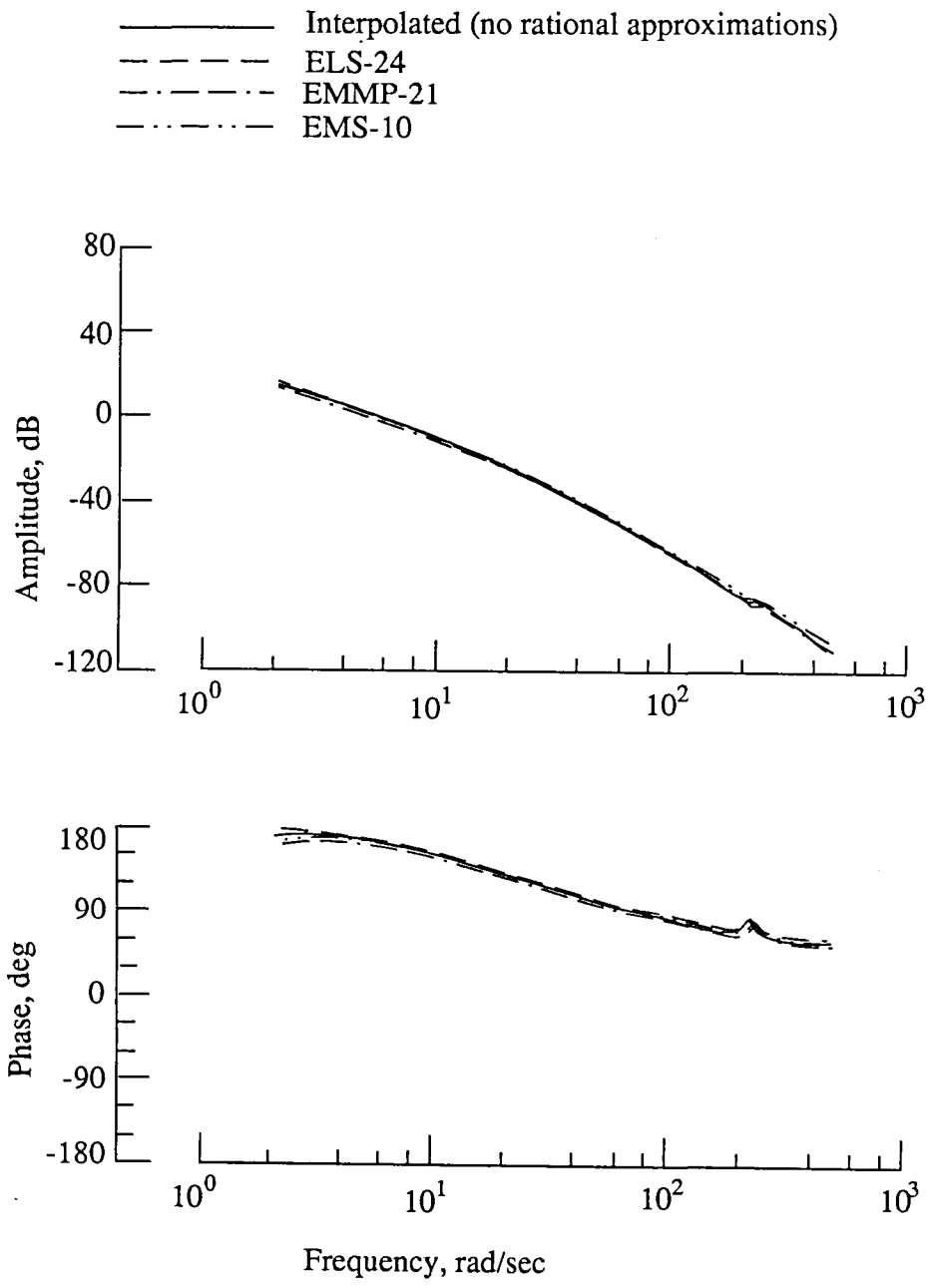

Figure 11. Comparison of pitch frequency response due to stabilizer deflection.

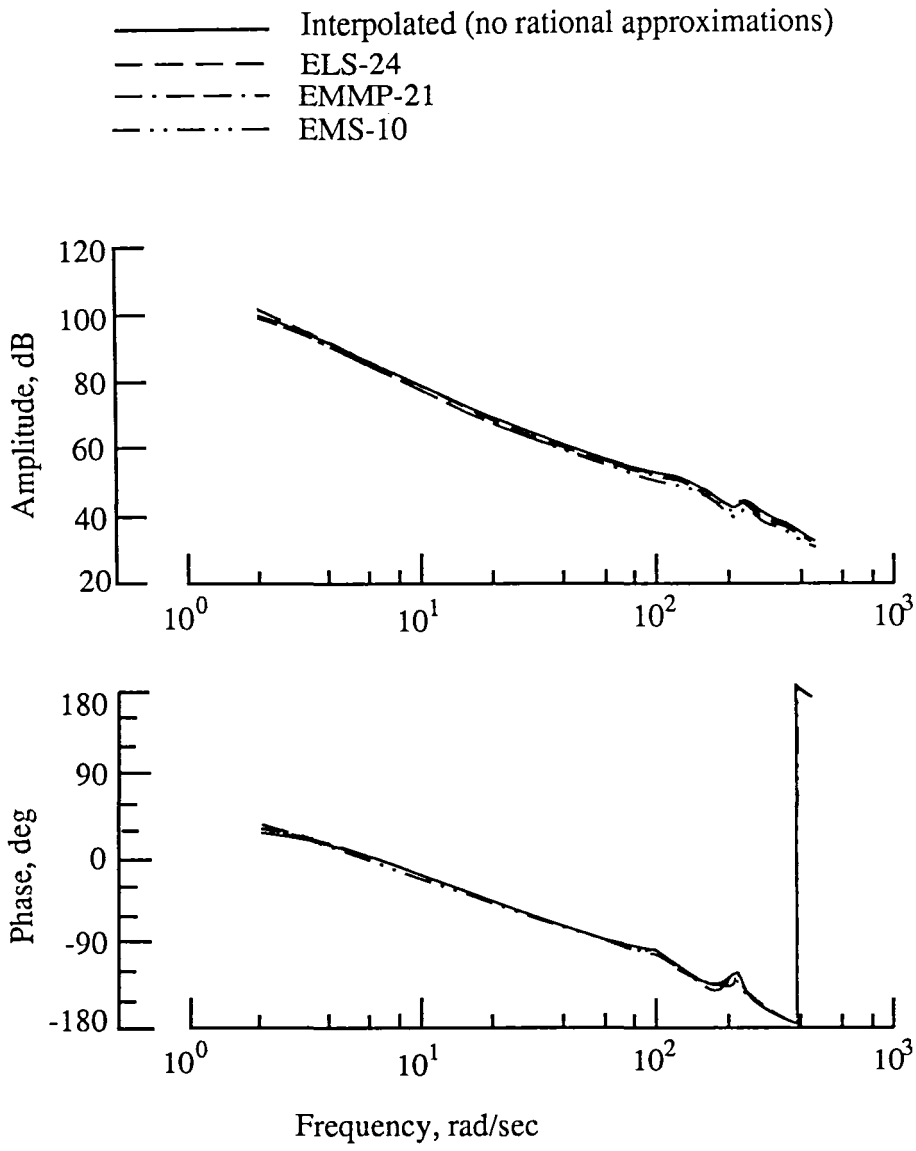

Figure 12. Comparison of c.g. acceleration frequency response due to stabilizer deflection.

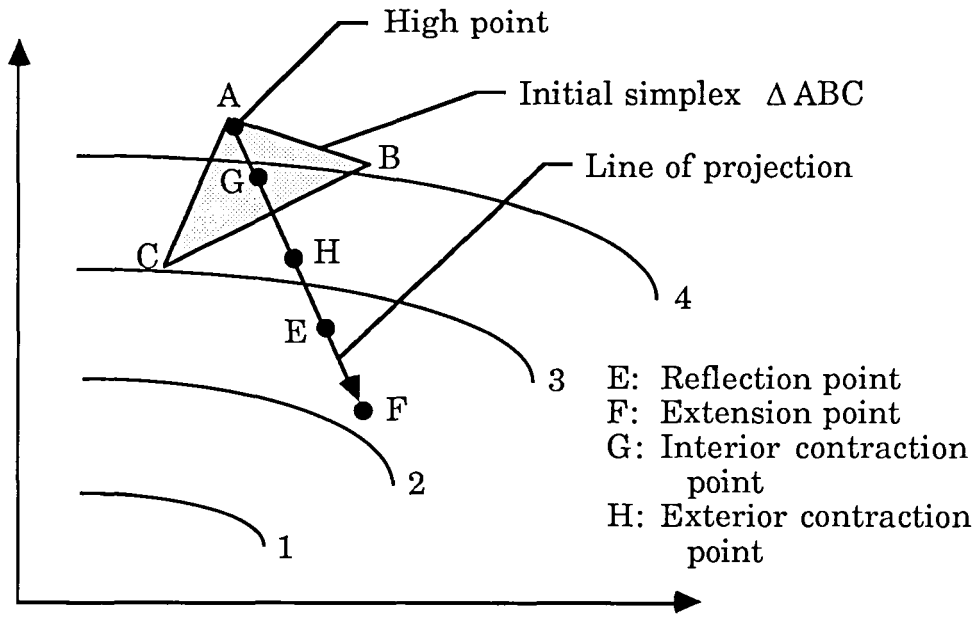

(a) Initial simplex and line of projection.

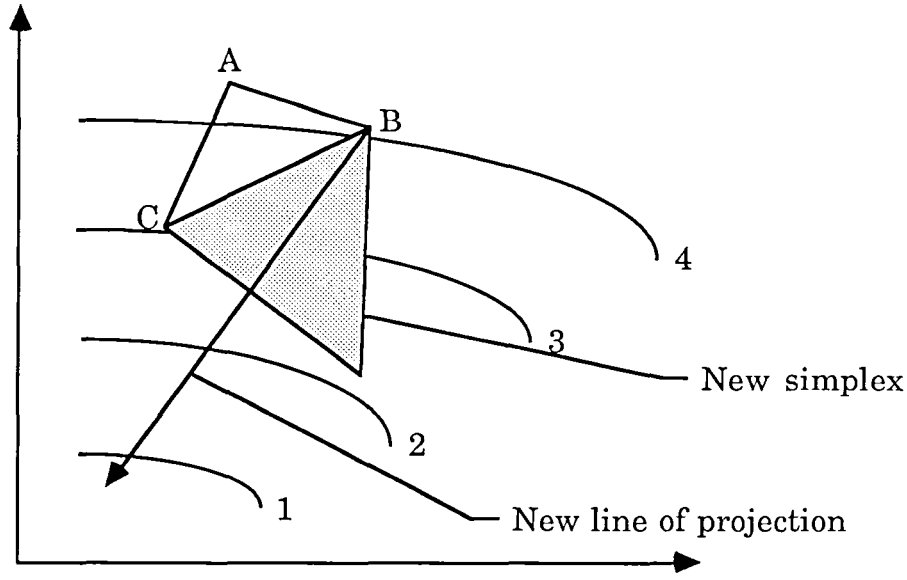

(b) New simplex and line of projection.

Figure 13. Two-dimensional view of adaptive sequential simplex algorithm.

NASA
National Aeronautics and Space Administration

Report Documentation Page

1. Report No.	2. Government Accession No.	3. Recipient's Catalog No.
NASA TP-2776		

4. Title and Subtitle	5. Report Date
Nonlinear Programming Extensions to Rational Function Approximation Methods for Unsteady Aerodynamic Forces	July 1988
	6. Performing Organization Code
7. Author(s)	8. Performing Organization Report No.
Sherwood H. Tiffany and William M. Adams, Jr.	L-16205
9. Performing Organization Name and Address	10. Work Unit No.
NASA Langley Research Center Hampton, VA 23665-5225	505-63-21-04
	11. Contract or Grant No.
12. Sponsoring Agency Name and Address	13. Type of Report and Period Covered
National Aeronautics and Space Administration Washington, DC 20546-0001	Technical Paper
	14. Sponsoring Agency Code

15. Supplementary Notes

16. Abstract

This paper deals with approximating unsteady generalized aerodynamic forces in the equations of motion of a flexible aircraft. Two methods of formulating these approximations are extended to include both the same flexibility in constraining the approximations and the same methodology in optimizing nonlinear parameters as another currently used "extended least-squares" method. Optimal selection of "nonlinear parameters" is made in each of the three methods by use of the same nonlinear, nongradient optimizer. The objective of the nonlinear optimization is to obtain rational approximations to the unsteady aerodynamic forces whose state-space realization is lower order than that required when the nonlinear terms are not optimized. The free "linear parameters" are determined using least-squares matrix techniques. Selected linear equality constraints are solved explicitly or included implicitly, using a Lagrange multiplier formulation. State-space mathematical models resulting from the different approaches are described, and comparative evaluations are presented from application of each of the extended methods to a numerical example. The results obtained for the example problem show that the number of differential equations used to represent the unsteady aerodynamic forces in linear time-invariant equations of motion can be significantly reduced (up to 67 percent) from the number required by a conventional method in which nonlinear terms are not optimized.

17. Key Words (Suggested by Authors(s))

s-plane approximation
Unsteady aerodynamics
First-order method
Minimum-state method
Least-squares method
ISAC
Matrix-Padé method

18. Distribution Statement

Unclassified—Unlimited

Subject Category 05

19. Security Classif.(of this report)	20. Security Classif.(of this page)	21. No. of Pages	22. Price
Unclassified	Unclassified	53	A04

For sale by the National Technical Information Service, Springfield, Virginia 22161-2171

National Aeronautics and
Space Administration
Code NTT-4

Washington, D.C.
20546-0001

NASA